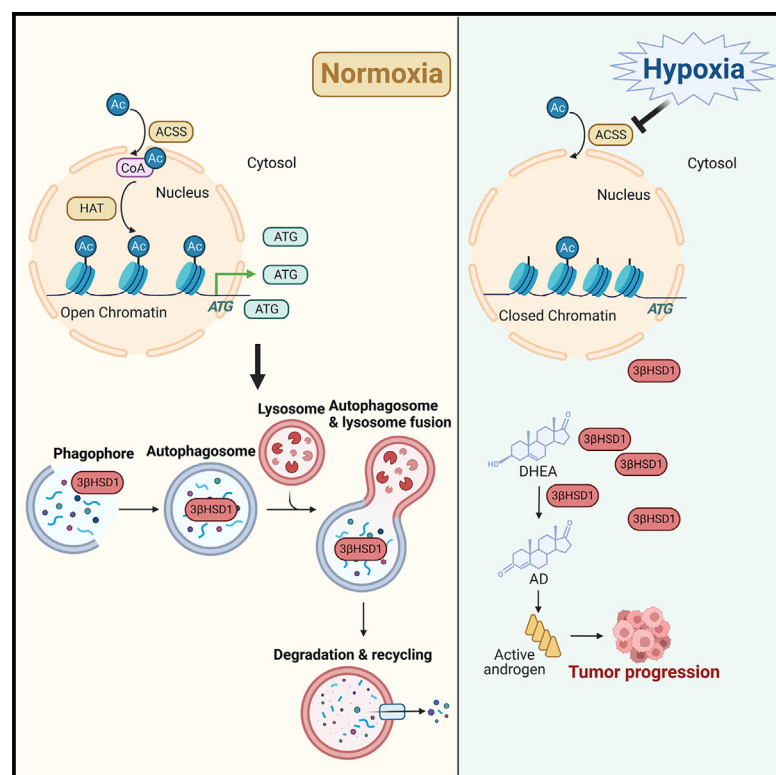


Chronic hypoxia stabilizes 3 β HSD1 via autophagy suppression

Graphical abstract



Authors

Liang Qin, Michael Berk, Yoon-Mi Chung, Di Cui, Ziqi Zhu, Abhishek A. Chakraborty, Nima Sharifi

Correspondence

nimasharifi@miami.edu

In brief

3 β HSD1 catalyzes the rate-limiting step of androgen synthesis in prostate cancer cells. Qin et al. show that chronic hypoxia upregulates adrenal-permissive 3 β HSD1(367T) by inhibiting its autophagy-mediated degradation. Chronic hypoxia represses the transcription of various autophagy-related (ATG) genes by decreasing histone acetylation to suppress autophagy.

Highlights

- Hypoxia stabilizes 3 β HSD1 protein by suppressing autophagy
- Autophagy inhibition promotes 3 β HSD1-dependent prostate cancer progression
- Hypoxia represses the transcription of ATG genes by decreasing histone acetylation
- Acetate promotes the transcription of ATG genes by increasing histone acetylation



Article

Chronic hypoxia stabilizes 3 β HSD1 via autophagy suppression

Liang Qin,^{1,2} Michael Berk,² Yoon-Mi Chung,^{2,5,6} Di Cui,¹ Ziqi Zhu,^{2,5,6} Abhishek A. Chakraborty,² and Nima Sharifi^{2,3,4,5,6,7,*}¹Department of Urology, Shanghai General Hospital, Shanghai Jiao Tong University School of Medicine, Shanghai 200080, China²Genitourinary Malignancies Research Center, Lerner Research Institute, Cleveland Clinic, Cleveland, OH 44195, USA³Department of Urology, Glickman Urological and Kidney Institute, Cleveland Clinic, Cleveland, OH 44195, USA⁴Department of Hematology and Oncology, Taussig Cancer Institute, Cleveland Clinic, Cleveland, OH 44195, USA⁵Desai Sethi Urology Institute, University of Miami Miller School of Medicine, Miami, FL 33136, USA⁶Sylvester Comprehensive Cancer Center, University of Miami Miller School of Medicine, Miami, FL 33136, USA⁷Lead contact*Correspondence: nimasharifi@miami.edu<https://doi.org/10.1016/j.celrep.2023.113575>

SUMMARY

Progression of prostate cancer depends on androgen receptor, which is usually activated by androgens. Therefore, a mainstay treatment is androgen deprivation therapy. Unfortunately, despite initial treatment response, resistance nearly always develops, and disease progresses to castration-resistant prostate cancer (CRPC), which remains driven by non-gonadal androgens synthesized in prostate cancer tissues. 3 β -Hydroxysteroid dehydrogenase/ $\Delta^5\rightarrow\Delta^4$ isomerase 1 (3 β HSD1) catalyzes the rate-limiting step in androgen synthesis. However, how 3 β HSD1, especially the “adrenal-permissive” 3 β HSD1(367T) that permits tumor synthesis of androgen from dehydroepiandrosterone (DHEA), is regulated at the protein level is not well understood. Here, we investigate how hypoxia regulates 3 β HSD1(367T) protein levels. Our results show that, *in vitro*, hypoxia stabilizes 3 β HSD1 protein by suppressing autophagy. Autophagy inhibition promotes 3 β HSD1-dependent tumor progression. Hypoxia represses transcription of autophagy-related (ATG) genes by decreasing histone acetylation. Inhibiting deacetylase (HDAC) restores ATG gene transcription under hypoxia. Therefore, HDAC inhibition may be a therapeutic target for hypoxic tumor cells.

INTRODUCTION

Prostate cancer is the most common malignancy in men and a major cause of cancer deaths in the United States.¹ The progression of prostate cancer is largely driven by the androgen receptor (AR) axis, which is activated by androgens, such as testosterone (T) and the more potent dihydrotestosterone (DHT).^{2,3} Therefore, androgen deprivation therapy (ADT) combined with chemotherapy or other hormonal agents that bring androgens down to castrate levels has been the mainstay treatment.⁴ However, drug resistance nearly always develops, and disease progresses to an advanced and lethal form, castration-resistant prostate cancer (CRPC).^{2,4,5} Similarly, although next-generation treatments, such as androgen synthesis inhibitors (e.g., abiraterone) or AR antagonists (e.g., enzalutamide, apalutamide, and darolutamide), are initially effective, resistance eventually develops. CRPC still relies on the AR axis, which in CRPC is activated by androgens synthesized from extragonadal precursor steroids.^{5–8} Thus, dehydroepiandrosterone (DHEA) and DHEA sulfate are the major precursor steroids for androgen synthesis in such circumstances.^{6–8} DHEA conversion to androstenedione (AD) is the rate-limiting step in androgen synthesis and is catalyzed by 3 β -hydroxysteroid dehydrogenase/ $\Delta^5\rightarrow\Delta^4$ isomerase (3 β HSD; Figure 1A), which is en-

coded by the *HSD3B1* gene.⁹ 3 β HSD exists as two isoforms, of which the 3 β HSD1 isoform is expressed in peripheral tissues such as the prostate, placenta, skin, and mammary gland.⁹

The ubiquitin-proteasome system and the autophagy-lysosome system are two major protein degradation pathways responsible for intracellular quality control.^{10,11} The ubiquitin-proteasome system degrades short-lived proteins, whereas the autophagy-lysosome system eliminates long-lived proteins, insoluble protein aggregates, and even whole organelles.^{10,11} Autophagy is driven by a conserved family of regulators, the autophagy-related (ATG) proteins.¹² Interestingly, some proteins, including AR and hypoxia-inducible factor 2 α (HIF2 α), can be degraded by both systems.^{13,14} We first reported 3 β HSD1 to be degraded by the ubiquitin-proteasome system, an event that is mediated by autocrine motility factor receptor (AMFR), an E3 ubiquitin ligase.¹⁵ Moreover, we identified a germline-encoded gain-of-function missense (N367T) in 3 β HSD1 that significantly stabilizes 3 β HSD1 protein.¹⁵ 3 β HSD1 stabilization increases androgen production, which promotes prostate cancer clinical progression after ADT.¹⁶ How 3 β HSD1(367T) is degraded is unknown, but clearly, understanding the mechanism underlying degradation of 3 β HSD1(367T) is important in identifying strategies to improve survival for patients.

Hypoxia, a hallmark of solid tumors, plays important roles in tumor progression, affecting multiple cellular events.¹⁷ The HIF



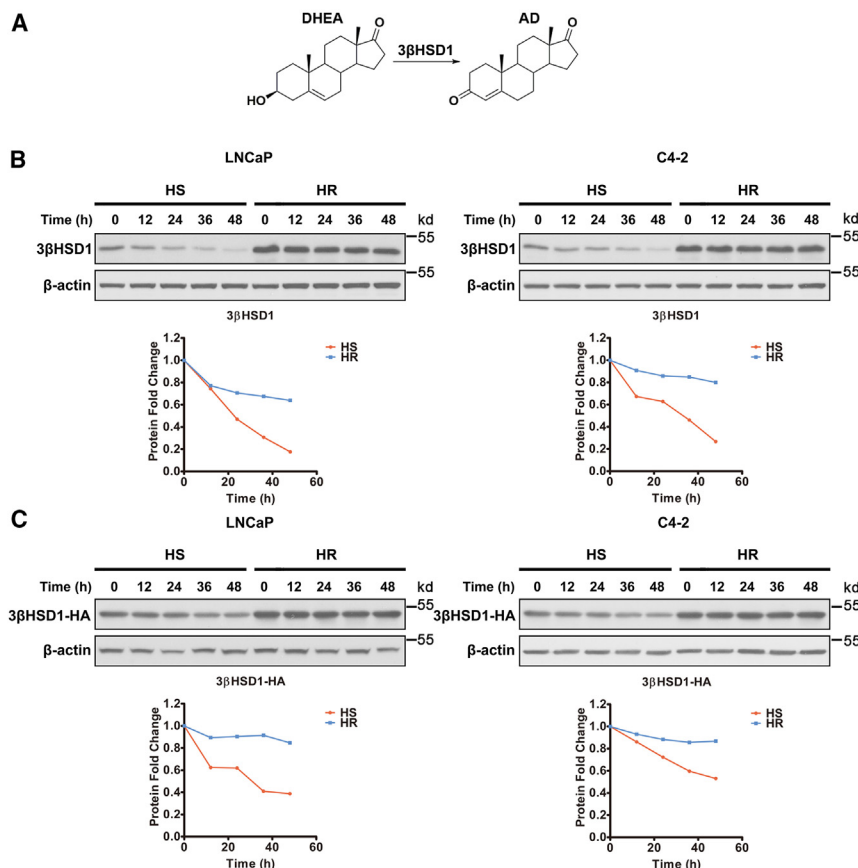


Figure 1. Chronic hypoxia stabilizes 3βHSD1(367T)

(A) The conversion from DHEA to AD. (B and C) The stability of endogenous 3βHSD1 (B) and overexpressed C-terminal HA-tagged 3βHSD1 (C) in HS cells under normoxia and HR cells under hypoxia was determined using a cycloheximide chase stability assay and western blot. Time 0 represents the point of cycloheximide (50 μM) addition. β-Actin was a loading control. All experiments were performed three times with equivalent results. The immunoblot images here are the representatives of the three assays, and the graphs are the quantification of these representatives. Western blot data were quantified by digital image analysis using ImageJ. HS, hypoxia sensitive; HR, hypoxia (chronic) resistant.

transcription factors are arguably the most prominent regulators of the cellular response to hypoxia.¹⁷ Functional HIF requires the association of an oxygen-sensitive α-subunit and an oxygen-insensitive β-subunit.¹⁷ Hypoxia prevents degradation of HIFα, thus resulting in its accumulation and dimerization with HIF1β, also called aryl hydrocarbon receptor nuclear translocator (ARNT), to induce the transcription of target genes.¹⁷ Moreover, hypoxia can regulate various cellular events via HIF-independent mechanisms.¹⁸

Hypoxia is recognized as a key driver in prostate cancer progression.^{19–28} However, how hypoxia affects androgen metabolism is poorly understood. Our previous study showed that hypoxia promotes transcription of *HSD3B1* via the EGLN1/VHL/HIF2α pathway.²⁹ HIF2α can directly bind the 5' regulatory region of *HSD3B1*.²⁹ Increased 3βHSD1 protein facilitates androgen production. Here, we demonstrate that chronic hypoxia significantly downregulates autophagy by decreasing the level of ATG mRNAs and proteins. Hypoxic suppression of autophagy leads to the stabilization of 3βHSD1 protein, thus defining an autophagy-dependent cellular mechanism that targets 3βHSD1(367T) for proteolysis.

RESULTS

3βHSD1(367T) is stabilized in HR cells under chronic hypoxia

Our previous study indicated that HIF2α can promote *HSD3B1* transcription by directly targeting its promoter region during

chronic hypoxia.²⁹ However, the 3βHSD1 protein level increased to a much greater extent than did the *HSD3B1* mRNA level.²⁹ Therefore, to further determine the mechanism of 3βHSD1 upregulation under chronic hypoxia, we determined whether chronic hypoxia also changes 3βHSD1 protein stability. Cellular protein synthesis was blocked by cycloheximide, and 3βHSD1 stability was monitored over time. The stability of both endogenous and hemagglutinin (HA)-tagged, overexpressed 3βHSD1 was measured in hypoxia-sensitive (HS) and hypoxia-resistant (HR) LNCaP and

C4-2 cells. Both endogenous and overexpressed 3βHSD1 were stabilized in HR cells under chronic hypoxia compared with HS cells under normoxia (Figures 1B and 1C).

3βHSD1(367T) is degraded via the autophagy-lysosome pathway

3βHSD1(367N) was reported to be degraded via AMFR-mediated ubiquitination, which is largely abolished by the N367T missense.¹⁵ Because both LNCaP and C4-2 cells express 3βHSD1(367T), we hypothesized that the observed 3βHSD1 stabilization in hypoxic cells likely occurs independently of ubiquitination-mediated degradation. To determine the mechanism of 3βHSD1(367T) degradation, we treated LNCaP and C4-2 cells with either a proteasome inhibitor (MG132) or lysosomal proteolysis inhibitors (bafilomycin A1 and chloroquine diphosphate salt). Interestingly, MG132 increased P62 slightly in LNCaP for an unknown reason but not in C4-2 at all (Figure 2A). MG132 increased conversion of LC3-I to LC3-II, an indicator of autophagy, since MG132 inhibited proteasome-mediated protein degradation, thus further inducing autophagy. Autophagy inhibitors suppressed the degradation of LC3-II. Therefore, both MG132 and autophagy inhibitors increased the ratio of LC3-II/LC3-I but in different mechanisms. The 3βHSD1(367T) level increased only when lysosomal activity was inhibited, which suggests that its degradation is mainly via the lysosome rather than the proteasome (Figure 2A). Next, we treated LNCaP and C4-2 cells with

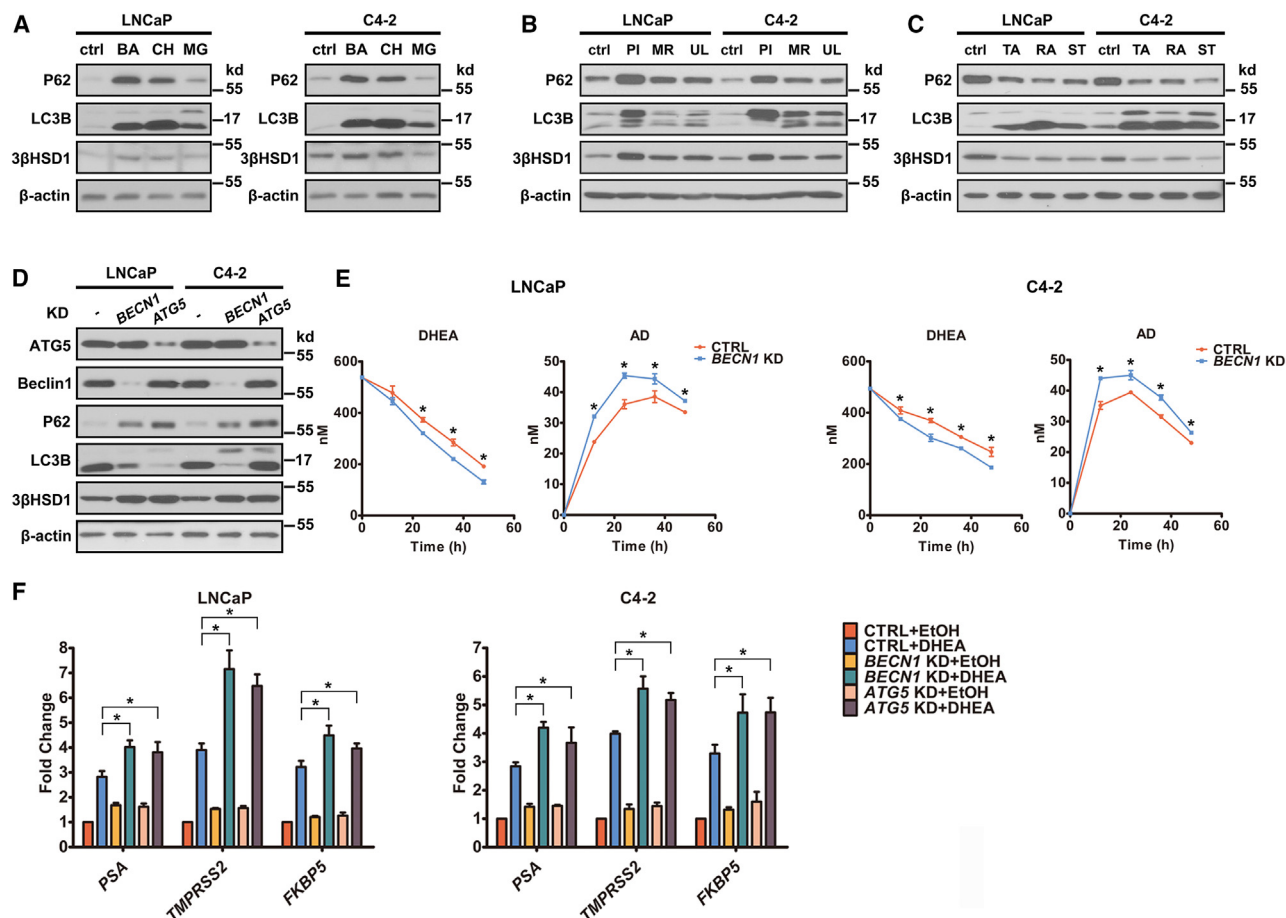


Figure 2. 3βHSD1(367T) is degraded via autophagy

(A) HS cells were treated with either a lysosome inhibitor, bafilomycin A1 (BA; 100 nM) or chloroquine diphosphate salt (CH; 50 μM) or a proteasome inhibitor, MG132 (MG; 10 μM). (B) HS cells were treated with one of three different autophagy inhibitors: PIK-III (PI; 5 μM), MRT68921 (MR; 1 μM), or ULK-101 (UL; 5 μM). The graphs are the quantification of the ratio of LC3-I/LC3-II in immunoblot images here by using ImageJ. (C) HS cells were treated with autophagy activators tat-beclin 1 (TA; 5 μM) or rapamycin (RA; 500 nM) or with serum starvation (ST) for 48 h. (D) *BECN1* or *ATG5* was stably knocked down by short hairpin RNA (shRNA) in HS cells. ATG5, Beclin 1, P62, LC3B, 3βHSD1, and β-actin proteins were determined by western blot. (E) DHEA and AD were quantified by mass spectrometry in LNCaP and C4-2 cells with *BECN1* stable knockdown and in the control cells shown in (D). Time 0 represents the point of DHEA addition. (F) AR-regulated transcripts were determined by qPCR in cells with *BECN1* or *ATG5* stable knockdown and in the control cells used in (D), with or without 8 h DHEA (50 nM) treatment. β-Actin was the loading control. *p < 0.05 using a one sample two-tailed t test. Error bars represent mean ± SEM.

autophagy inhibitors that target different steps of autophagy (Figure S1). PIK-III is a selective inhibitor of VPS34 enzymatic activity with an IC₅₀ of 18 nM.³⁰ MRT68921 is a potent and dual ULK1/2 inhibitor with IC₅₀ values of 2.9 and 1.1 nM, respectively.³¹ ULK-101 is a dual inhibitor of ULK1/2 with IC₅₀ values of 8.3 and 30 nM, respectively.³² ULK1/2 leads to activation of the Beclin 1-VPS34 complex, which then promotes autophagy by forming phosphatidylinositol 3-phosphate on membranes mainly from the endoplasmic reticulum.¹² Treatment with any of these inhibitors significantly increased the level of P62, indicating that autophagy was inhibited (Figure 2B). Our study showed that all treatment increased the level of both LC3-I and LC3-II (Figure 2B). Combined with P62 result, this suggests that autophagy-mediated degradation of LC3-II is inhibited. PIK-III significantly increased

the level of LC3-I as well as the ratio of LC3-I/LC3-II, but MRT68921 and ULK-101 increased both LC3-I and LC3-II almost equally (Figure 2B). This difference may be attributed to their different mechanisms of autophagy inhibition, as PIK-III is a selective inhibitor of VPS34, whereas MRT68921 and ULK-101 are dual inhibitors of ULK1/2. Treatment also increased 3βHSD1, and PIK-III exhibited the most potent effect (Figure 2B).

We then induced autophagy by targeting different pathways (Figure S1). Tat-beclin 1 is a peptide that interacts with the negative regulator of Beclin 1 to release Beclin 1 from the Golgi. Rapamycin inhibits mTOR, a kinase that phosphorylates and inactivates ULK1/2. Starvation elevates the ratio of AMP/ATP to activate AMPK, which also inhibits mTOR activity. The reductions in P62 and ratio of LC3-I to LC3-II indicate that all these treatments

induced autophagy (Figure 2C). 3 β HSD1 was also decreased by all three treatments (Figure 2C). Moreover, the knockdown of either *BECN1* or *ATG5* inhibited autophagy and increased 3 β HSD1 (Figure 2D). *BECN1* knockdown accelerated the conversion of DHEA to AD (Figure 2E). DHEA-induced AR target gene expression was also enhanced by the knockdown of either *BECN1* or *ATG5* (Figure 2F). These data together suggest that 3 β HSD1(367T) is degraded via the autophagy-lysosome pathway, unlike 3 β HSD1(367N), which is degraded via the ubiquitin-proteasome system. Compared to short-lived proteins that are degraded by the proteasome, 3 β HSD1(367T) exhibited a relatively longer half-life (more than 16 h; Figures 1B and 1C), which also suggests autophagy-dependent degradation.

3 β HSD1(367T) is degraded via macroautophagy, not microautophagy or chaperone-mediated autophagy

Three autophagy mechanisms have been reported: macroautophagy, microautophagy, and chaperone-mediated autophagy. 3 β HSD1 upregulation by VPS34 and ULK1/2 inhibition suggests that 3 β HSD1(367T) is degraded via macroautophagy because VPS34 and ULK1/2 are involved only in macroautophagy (Figure 2B).³³ Indeed, 3-methyladenine, another VPS34 inhibitor, can also increase 3 β HSD1(367T) in LNCaP and C4-2 cells (Figure S2A). Next, we tested whether the other two types of autophagy are also involved in 3 β HSD1(367T) degradation. Microautophagy recognizes cytosolic cargo bound to heat shock protein family A (Hsp70) member 8 (HSPA8) and then moves the cargo into small vesicles formed by direct lysosomal membrane invagination.³³ Chaperone-mediated autophagy targets KFERQ-like motif-bearing proteins for degradation via the interaction of chaperone HSPA8 and lysosome-associated membrane protein type 2A (LAMP2A), which shuttles the cargo into the lysosome.³³ Therefore, HSPA8 is required for both microautophagy and chaperone-mediated autophagy, but LAMP2A is only required for chaperone-mediated autophagy. Neither *LAMP2* nor *HSPA8* knockdown increased the 3 β HSD1(367T) level (Figure S2B). Moreover, neither *LAMP2* nor *HSPA8* overexpression decreased 3 β HSD1(367T) (Figure S2C). Collectively, these data suggest that microautophagy and chaperone-mediated autophagy are not responsible for degradation of 3 β HSD1(367T).

Autophagy inhibition promotes 3 β HSD1-dependent tumor progression

To determine the role of autophagy in prostate tumorigenesis, specifically its dependence on 3 β HSD1, we stably knocked down *BECN1* to decrease autophagy activity in both *HSD3B1*-proficient and -deficient C4-2 cells. *BECN1* knockdown increased 3 β HSD1 protein (Figure 3A) and promoted cell proliferation *in vitro*, which largely depended on 3 β HSD1 (Figure 3B). PIK-III, a selective inhibitor of VPS34, also promoted cell proliferation in a 3 β HSD1-dependent manner (Figure S3A). A xenograft study in surgically orchiectomized mice showed that *BECN1* knockdown promoted tumorigenesis *in vivo*, which also largely depended on 3 β HSD1 (Figures 3C and 3D). These data suggest that inhibiting autophagy increases 3 β HSD1 protein levels to promote CRPC. We next analyzed androgen levels in these tumor samples by mass spectrometry. *BECN1* knockdown significantly increased the synthesis of active androgens, such as T

and DHT, which is dependent on 3 β HSD1 (Figure 3E). Interestingly, the ratio of AD/DHEA was not altered after *BECN1* knockdown (Figure S3B). The reason could be the much faster conversion of AD to downstream metabolites such as T and 5 α -dione compared to the much slower conversion of DHEA to AD, a rate-limiting step of androgen synthesis. This is supported by the much smaller value of AD/DHEA ratio compared to the (T+DHT)/DHEA ratio (Figures 3E and S3B).

Autophagy is not involved in regulating DHEA conversion to AD in LAPC4 cells

To determine whether the cells with 3 β HSD1(367N) are also affected by autophagy suppression, we knocked down *BECN1* in LAPC4 cells in which 3 β HSD1(367N) is expressed. We compared the conversion of DHEA to AD as well as DHEA-dependent cell growth in both *BECN1* knockdown cells and control cells. Our results indicated that *BECN1* knockdown did not alter the conversion of DHEA to AD (Figure S4A) or the proliferation of LAPC4 (Figure S4B). *HSD3B1* knockout significantly inhibited the proliferation of LAPC4, indicating the critical role of DHEA metabolism in promoting LAPC4 proliferation (Figure S4B). Together, these data suggest that the degradation of 3 β HSD1(367N) is not mediated by autophagy.

HR cells exhibit reduced autophagy under chronic hypoxia

Because HR cells exhibited stabilized 3 β HSD1(367T) (Figure 1), which was degraded via the autophagy-lysosome pathway (Figure 2), we hypothesized that autophagy is downregulated in HR cells. To compare the autophagy level in HS and HR cells, we stably overexpressed OFPspark-LC3 in both HS and HR cells, which allowed us to determine the autophagy level by quantifying LC3 puncta. Serum starvation (48 h) led to fewer LC3 puncta in HR cells than in HS cells (Figure 4A). Such decreased autophagy might explain the stabilization of 3 β HSD1(367T) in HR cells. We also compared the autophagy level between HS and HR cells by determining the ratio of LC3-I to LC3-II. HR cells exhibited a markedly increased ratio of LC3-I to LC3-II, indicating a much lower autophagy level (Figure 4B). Moreover, we also performed lactate dehydrogenase (LDH) sequestration assay to compare the autophagy levels between HS and HR cells by determining the sequestration of LDH by the cells. The result (Figure S5) is consistent with the result of LC3 fluorescence (Figure 4A), suggesting the decreased autophagy exhibited by HR cells compared to HS cells. These data together suggest that autophagy is downregulated in HR cells under chronic hypoxia, which decreases autophagy-mediated degradation of 3 β HSD1(367T). To investigate the mechanism of decreased autophagy in HR cells under chronic hypoxia, we compared the level of key autophagy regulators in both HS and HR cells. A panel of 19 ATG genes were analyzed at the protein (Figure 4B) and mRNA levels (Figure 4C). Surprisingly, most of these autophagy regulators were significantly decreased at the protein level in HR cells. Some differences were observed between LNCaP and C4-2 cells: for LNCaP cells, ATG5, ATG3, and WIPI2 protein did not differ between HR and HS cells; in contrast, for C4-2 cells, these protein levels were lower in HR cells (Figure 4B). LC3A was increased in HR LNCaP but decreased in

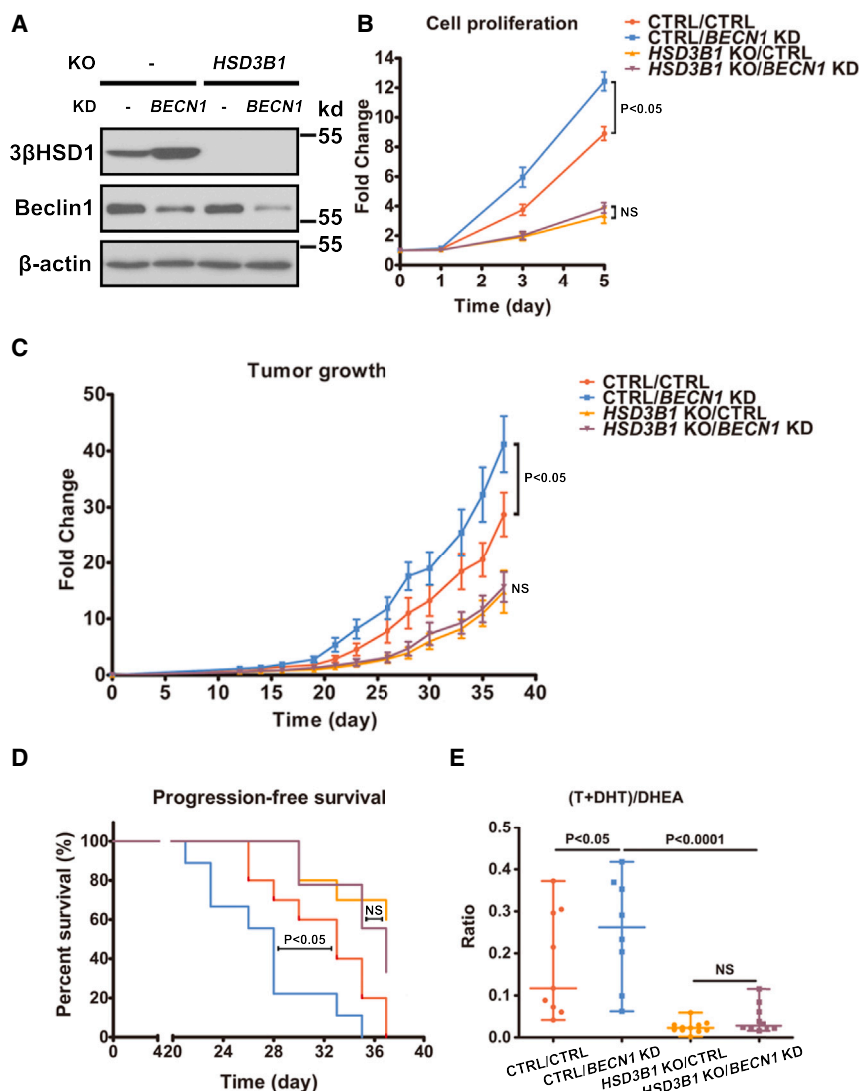


Figure 3. In vivo analysis of tumors with BECN1 knockdown

(A) 3βHSD1 and Beclin 1 protein expression in HSD3B1 knockout (KO) and control C4-2 cells with and without shRNA-mediated BECN1 stable knockdown was determined by western blot. β-Actin was the loading control.

(B) The proliferation of the cells in (A) was measured by luciferase assay. The cells were treated with DHEA (50 nM) from time 0. The proliferation was compared using an unpaired two-tailed t test on day 5.

(C–E) The cells in (A) were used in a xenograft study with DHEA treatment after castration. Castration and DHEA pellet implantation were performed when the tumor volume reached 100 mm³. The number of mice in the control (CTRL)/CTRL, CTRL/BECN1 knockdown (KD), HSD3B1 KO/CTRL, and HSD3B1 KO/BECN1 KD groups were 9, 10, 11, and 10, respectively, in (C) and (D) but 9, 8, 11, and 10 in (E), in which two outliers were excluded from the CTRL/BECN1 KD group.

(C) Change in tumor volume was measured, and the tumor volume on day 37 was compared using an unpaired two-tailed t test.

(D) Progression-free survival was assessed as time from cell injection to tumor volume of 500 mm³ and compared using a log rank (Mantel-Cox) test.

(E) T, DHT, and DHEA were measured in xenograft tumor samples from (C) using mass spectrometry, and the ratio of (T+DHT)/DHEA is shown for each xenograft group. Error bars represent mean ± SEM. The Mann-Whitney test was used to calculate a two-tailed p value, $p = 0.0434$.

Cycloheximide was used to terminate global protein synthesis. Interestingly, our results suggested that the protein stability of most autophagy regulators was not altered in HR cells as compared to HS cells (Figure S6). These regulators exhibited a

long half-life, except for ULK1, ATG13, ATG10, and LC3A/B-II. LC3A and LC3B were degraded even more slowly in HR cells as compared to HS cells (Figure S6), mainly due to the reduced autophagy during which LC3 is degraded as part of the cargo, which was consistent with the lower level of autophagy in HR cells (Figure 4A). However, stability of another ATG8 family member, GABARAP, was similar between HS and HR cells. Moreover, the membrane-bound form of GABARAP (GABARAP II, lower band; Figure S6) was degraded much more rapidly than the unbound form (GABARAP I, upper band) for an unknown reason. Previous research suggests that hypoxia increases the phosphorylation of eIF2α, which inhibits initiation of mRNA translation.³⁴ We compared the overall protein synthesis rates between HS cells under normoxia and HR cells under hypoxia. HR cells exhibited a striking decrease in global protein translation compared to HS cells (Figure S7), which is consistent with previous studies.³⁴ Therefore, because autophagy regulator protein stability is not altered in HR cells, it is possible that the decrease in global protein synthesis contributes to regulator downregulation.

HR C4-2 cells. Compared with LNCaP cells, C4-2 cells exhibited a higher ratio of LC3-I to LC3-II, which indicates a lower level of autophagy (Figure 4B). In contrast to most of the other autophagy regulators, ATG9A was increased in both HR LNCaP and HR C4-2 cells (Figure 4B). Then, we determined whether the altered protein level of these autophagy regulators is due to changes in mRNA level. Interestingly, although the change in the mRNA expression level of many autophagy regulators was consistent with their protein level change, this was not consistent across all regulators, suggesting that the protein downregulation does not occur via decreased transcription or greater RNA decay (Figures 4C and 4D).

The stability of autophagy regulators is not altered in HR cells

Because the decrease in some autophagy regulators in HR cells was not due to their mRNA downregulation, we determined whether their protein stability was altered. Protein stability was compared in HS cells under normoxia and HR cells under hypoxia.

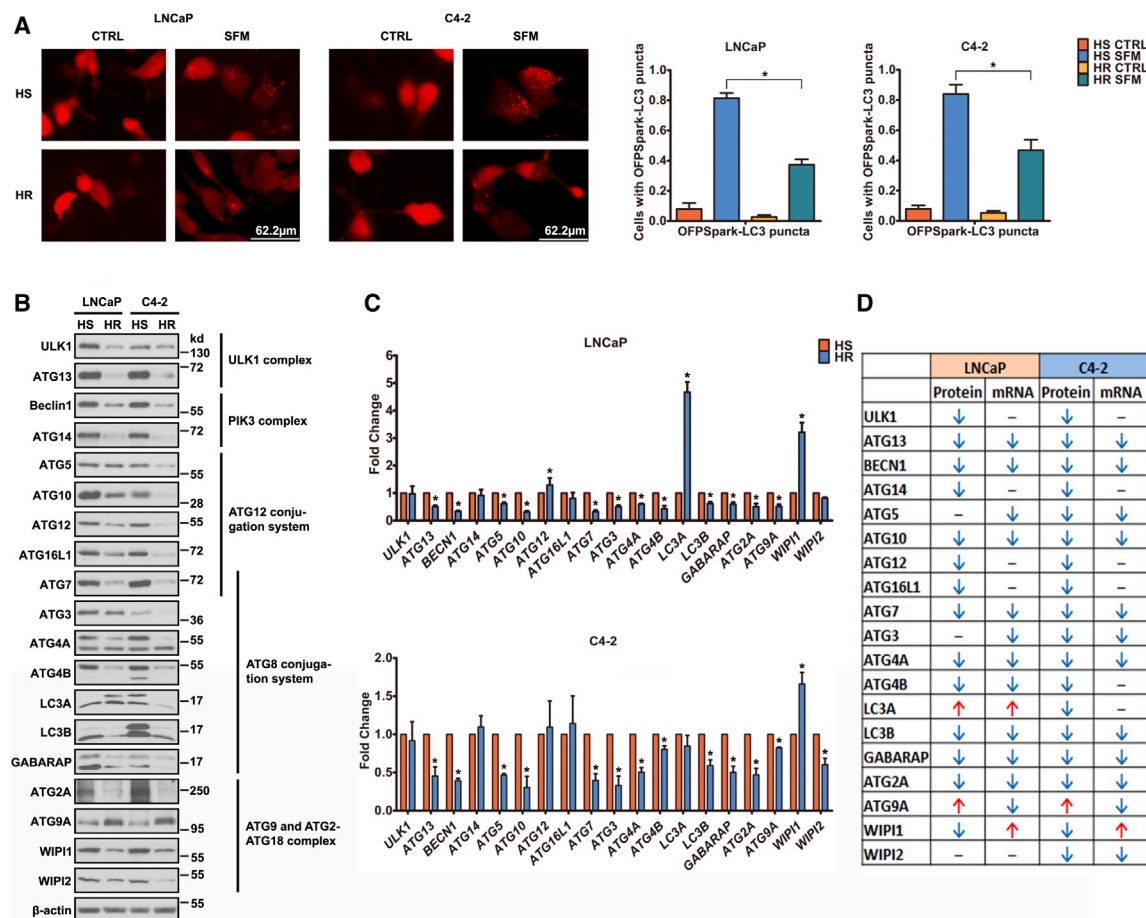


Figure 4. Autophagy level is reduced in HR cells under chronic hypoxia

(A) Both HS and HR cells that stably expressed OFPSpark-LC3 were treated with either normal media (CTRL) or starved with serum-free media (SFM) from 48 h. Representative microscopy images of LC3 staining are shown. The images were taken at 40 \times , and the scale bars represent 62.2 μ m. The bar chart shows the percentages of autophagic cells, which were calculated as the number of cells with more than 10 OFPSpark-LC3 puncta divided by the total number of OFPSpark-positive cells in the same field. Quantification was performed from 3 independent experiments with >25 cells using ImageJ quantification.

(B and C) Protein (B) and mRNA (C) were determined by western blot and qPCR, respectively, for the indicated autophagy regulators and β -actin in HS cells under normoxia and HR cells under hypoxia. β -Actin was the loading control. * p < 0.05 using a one sample two-tailed t test. Error bars represent mean \pm SEM.

(D) Summary of results in (B) and (C).

Histone methylation is increased, but histone acetylation is decreased, in HR cells under chronic hypoxia

Hypoxia regulates targeted gene expression via both HIF-dependent and HIF-independent mechanisms. HIF has been reported to be involved in gene expression promotion but not repression.³⁵ Therefore, we determined whether the repressed transcription of the autophagy regulators in HR cells is due to HIF-independent mechanisms, such as altered histone modification. Hypoxia has been reported to increase histone methylation and decrease histone acetylation.^{36,37} Indeed, our results confirmed that H3K9 methylation was increased, but H3K9 and H3K27 acetylation was decreased, in HR cells under chronic hypoxia (Figure S8A). Interestingly, these histone modifications were reversible in HR cells: upon reoxygenation, they quickly reverted to the modification status seen in HS cells under normoxia (Figure S8B). After incubating these HR cells for 7 days under normoxia, we trans-

ferred them back to hypoxia. Again, these histone modifications quickly reverted to modification levels seen before transfer to normoxia (Figure S8B). A short-term assay suggested that these histone modifications started to gradually revert to those seen in HS cells under normoxia after 6 h reoxygenation (Figure S8C).

The repressed transcription of autophagy regulators is not due to increased histone methylation in HR cells

Because histone methylation contributes to repression of numerous genes,^{38,39} we determined whether the increased histone methylation in HR cells is responsible for the repressed expression of autophagy regulators. HR cells were treated with two histone methyltransferase G9a/GLP inhibitors: UNC0642, with an IC₅₀ less than 2.5 nM,⁴⁰ and A-366, with an IC₅₀ of 3.3 nM.⁴¹ Both inhibitors significantly decreased H3K9 methylation (Figure S9A). However, neither inhibitor altered the expression of autophagy regulators, suggesting that the repressed

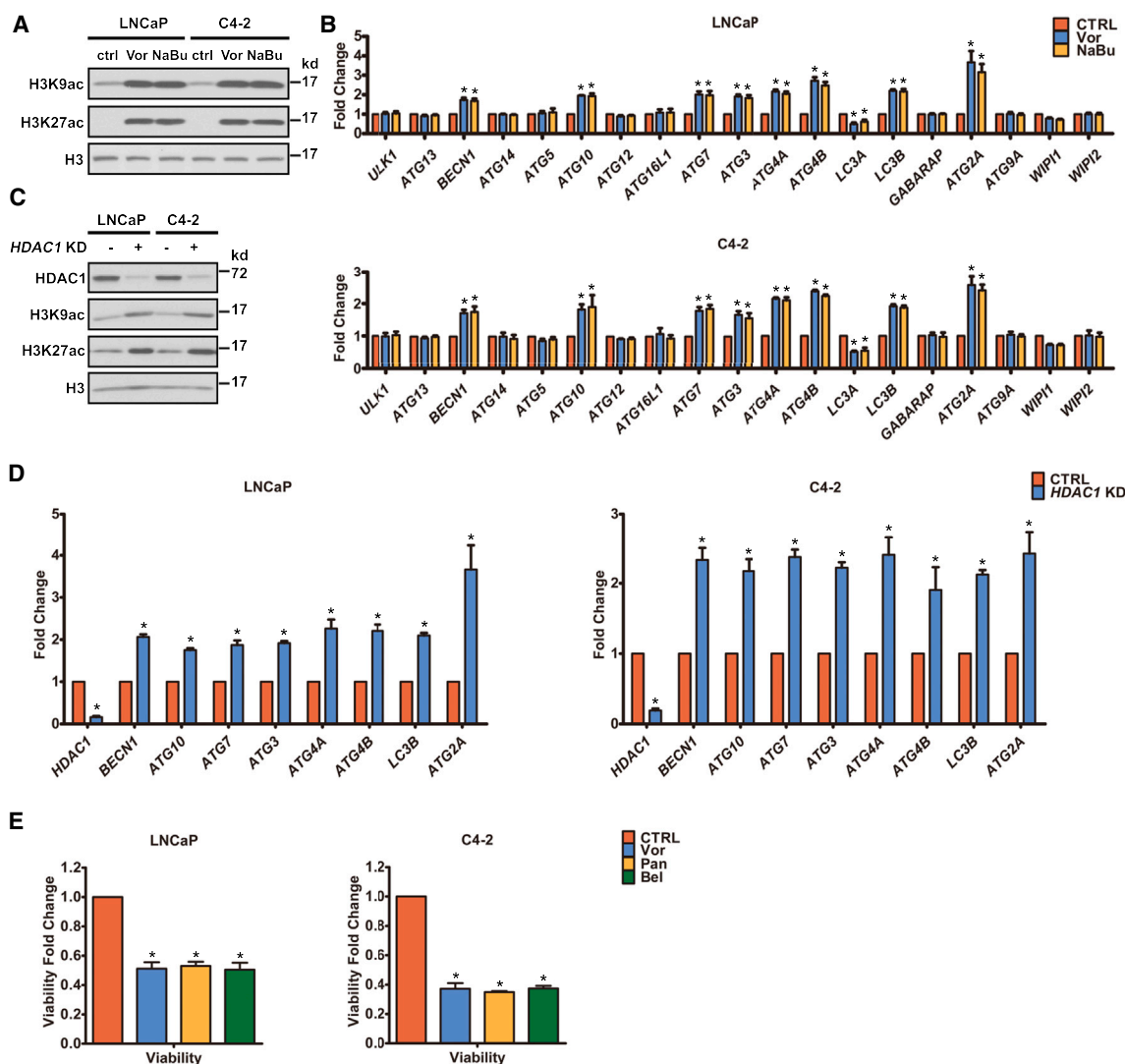


Figure 5. Decreased histone acetylation downregulates autophagy regulator mRNA

(A and B) Both HR LNCaP and C4-2 cells were treated with an HDAC inhibitor, either vorinostat (Vor; 10 μ M) or sodium butyrate (NaBu; 5 mM) for 36 h under hypoxia.

(A) H3K9ac, H3K27ac, and H3 proteins were determined by western blot. H3 was the loading control.

(B) mRNA level was determined by qPCR for the indicated autophagy regulators.

(C and D) *HDAC1* was stably knocked down by shRNA in HS cells.

(C) HDAC1, H3K9ac, H3K27ac, and H3 proteins were determined by western blot. H3 was the loading control.

(D) *HDAC1*, *BECN1*, *ATG10*, *ATG7*, *ATG3*, *ATG4A*, *ATG4B*, *LC3B*, and *ATG2A* mRNA was determined by qPCR. *ACTB* was the loading control. *p < 0.05 using a one sample two-tailed t test.

(E) HR cells were treated with either DMSO (CTRL), Vor (20 μ M), panobinostat (Pan; 1 μ M), or belinostat (Bel; 5 μ M) for 48 h under hypoxia. Cell viability was measured using a luciferase assay (Promega). *p < 0.05 using an unpaired two-tailed t test. Error bars represent mean \pm SEM.

transcription of autophagy regulators in HR cells is not due to increased histone methylation (Figure S9B).

Decreased histone acetylation in HR cells contributes to the repressed transcription of autophagy regulators

Considering that histone acetylation promotes the transcription of numerous genes,³⁸ we also determined whether the decreased histone acetylation in HR cells is responsible for the repressed expression of autophagy regulators. HR cells were treated with

two histone deacetylase (HDAC) inhibitors: vorinostat, with an IC₅₀ of 10 nM,⁴² or sodium butyrate, with IC₅₀ values of 0.3, 0.4, and 0.3 mM for HDAC1, -2, and -7, respectively.⁴³ HDAC inhibition significantly increased both H3K9 and H3K27 acetylation (Figure 5A). Both inhibitors elevated mRNA expression of several autophagy regulators, suggesting the repressed transcription of some autophagy regulators in HR cells is due to decreased histone acetylation (Figure 5B). We compared the protein and mRNA levels of all HDACs in HS and HR cells. Interestingly, HR

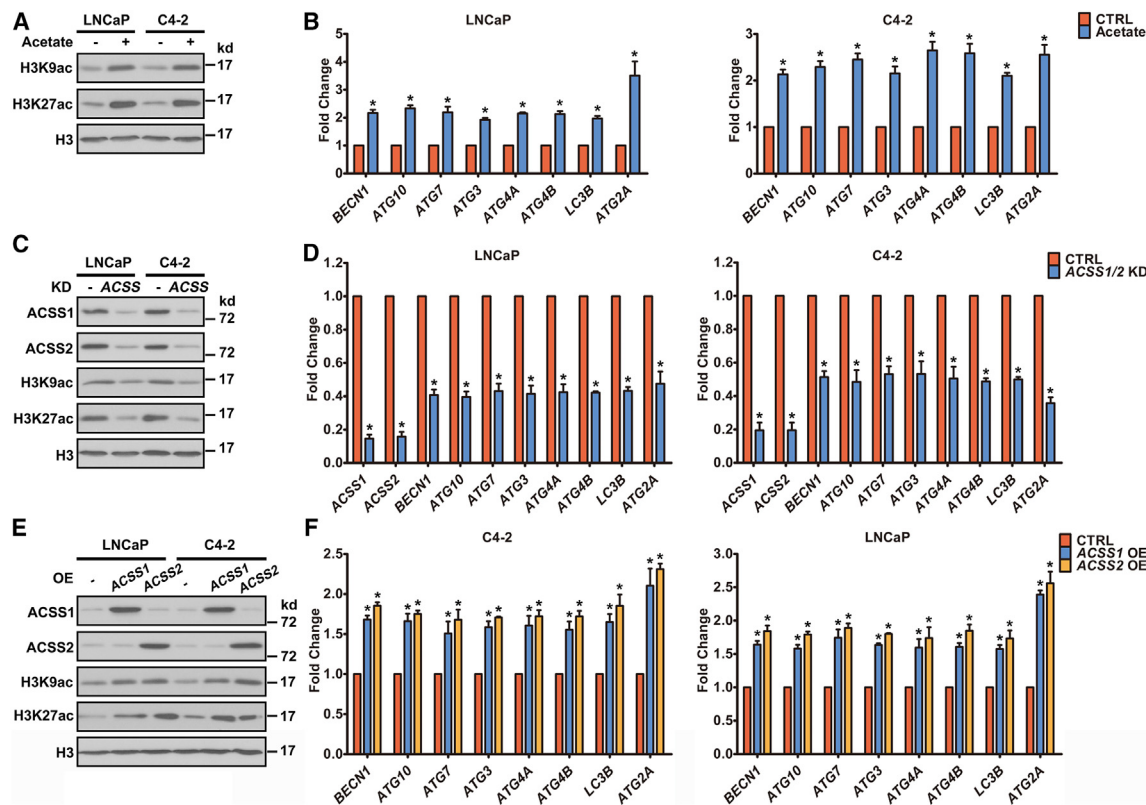


Figure 6. Acetate metabolism regulates histone-acetylation-mediated transcription of autophagy regulators

(A and B) HR LNCaP and C4-2 cells were treated with acetate (5 mM) for 24 h under hypoxia. (A) H3K9ac, H3K27ac, and H3 proteins were determined by western blot. H3 was the loading control. (B) *BECN1*, *ATG10*, *ATG7*, *ATG3*, *ATG4A*, *ATG4B*, *LC3B*, and *ATG2A* mRNA was determined by qPCR. *ACTB* was the loading control. (C and D) Both *ACSS1* and *ACSS2* were stably knocked down by shRNA in HR cells. (C) *ACSS1*, *ACSS2*, H3K9ac, H3K27ac, and H3 proteins were determined by Western blot. H3 was the loading control. (D) *ACSS1*, *ACSS2*, *BECN1*, *ATG10*, *ATG7*, *ATG3*, *ATG4A*, *ATG4B*, *LC3B*, and *ATG2A* mRNA was determined by qPCR. (E and F) *ACSS1* or *ACSS2* was overexpressed in HR cells. (E) *ACSS1*, *ACSS2*, H3K9ac, H3K27ac, and H3 proteins were determined by western blot. H3 was the loading control. (F) *BECN1*, *ATG10*, *ATG7*, *ATG3*, *ATG4A*, *ATG4B*, *LC3B*, and *ATG2A* mRNA was determined by qPCR. *ACTB* was the loading control. * $p < 0.05$ using a one sample two-tailed t test. Error bars represent mean \pm SEM.

C4-2 cells exhibited a decreased protein level for all HDACs except HDAC1, and HR LNCaP cells also exhibited a decreased protein level for most HDACs except HDAC1, HDAC5, and HDAC9 (Figures S10A and S10C). The changes of some HDAC mRNAs were not consistent with their protein-level changes (Figures S10B and S10C). As HDAC1 protein level remained unchanged in both HR LNCaP and C4-2 cells, we hypothesized that it is the major HDAC that functions under hypoxia, thus stably knocking down *HDAC1* in HR cells. *HDAC1* knockdown also markedly increased H3K9 and H3K27 acetylation (Figure 5C), as well as the expression of several autophagy regulators that had also been elevated by HDAC inhibitors (Figure 5D). Several HDAC inhibitors have been tested to treat patients with prostate cancer.^{44–46} To determine the effect of HDAC inhibitors on HR cell viability, we treated HR cells with various HDAC inhibitors, and our results showed that all of them resulted in a great loss of cell viability, at least in part by elevating the autophagic response in oxygen-deprived cells (Figure 5E).

Acetate promotes the transcription of autophagy regulators via increasing histone acetylation

Hypoxia was reported to induce histone hypoacetylation by reducing acetyl-CoA generation.^{47,48} Acetate supplementation can promote gene transcription by increasing histone acetylation to restore chromatin accessibility during hypoxia.^{47,48} Therefore, we determined whether acetate can regulate histone acetylation and the expression of autophagy regulators. Acetate significantly increased both H3K9 and H3K27 acetylation (Figure 6A), as well as the mRNA level of the autophagy regulators (Figure 6B). Two enzymes are mainly responsible for acetyl-CoA production from acetate in mammals: *ACSS1* in mitochondria and *ACSS2* in cytosol.⁴⁹ The expression of both *ACSS1* and *ACSS2* was decreased in HR cells under chronic hypoxia (Figures S11A and S11B). To determine which isoform is responsible for mediating the acetate-induced increase in histone acetylation, we knocked down *ACSS1* and *ACSS2* individually. Interestingly, our results showed that knockdown of either *ACSS1* or *ACSS2* individually

abolishes neither the acetate-induced increase in H3K9 and H3K27 acetylation (Figure S11C) nor the increase in mRNA level of the autophagy regulators (Figure S11D), indicating the redundant roles played by ACSS1 and ACSS2. This observation is consistent with a previous study.⁴⁸ Therefore, we then stably knocked down both ACSS1 and ACSS2 in HR cells. Our results showed that ACSS1/2 double knockdown inhibited acetate-induced increase in H3K9 and H3K27 acetylation (Figure 6C), as well as the increased mRNA level of the autophagy regulators (Figure 6D). The overexpression of either ACSS1 or ACSS2 individually promoted the acetate-induced increase in H3K9 and H3K27 acetylation (Figure 6E), and the increase in the mRNA level of the autophagy regulators (Figure 6F), also indicating the redundant roles played by ACSS1 and ACSS2.

DISCUSSION

The growth of prostate cancer cells largely depends on the activation of AR by androgens such as T and DHT.^{2,5,50} Multiple clinical studies have shown that CRPC relies on intratumoral androgens that are synthesized from precursors such as DHEA in peripheral tumor tissues, suggesting the critical role of intratumoral androgen synthesis in CRPC.^{5,6,51,52} Preclinical studies indicate that hypoxia promotes both local aggressiveness and metastasis of prostate cancer.^{19–28} Therefore, understanding the mechanisms that alter androgen synthesis with hypoxia is important for the development of more effective treatments. However, how hypoxia affects androgen metabolism in prostate cancer is not well understood. 3 β HSD1 catalyzes the rate-limiting reaction in androgen synthesis from extragonadal precursor steroids.⁹ We previously showed that hypoxia promotes transcription of *HSD3B1* via the EGLN1/VHL/HIF2 pathway.²⁹ Our findings here suggest that in addition to increasing *HSD3B1* transcription, hypoxia can elevate 3 β HSD1 protein levels by decreasing autophagy-mediated degradation of 3 β HSD1: chronic hypoxia significantly downregulated ATG expression by reducing histone acetylation.

We first identified a gain-of-function missense (N367T) in 3 β HSD1 that stabilizes the protein via abolishing its proteasome-mediated degradation, and AMFR, an E3 ubiquitin ligase, was responsible for the ubiquitination of 3 β HSD1(367N).¹⁵ However, how 3 β HSD1(367T), with a longer half-life relative to 3 β HSD1(367N), is eventually degraded was unknown. 3 β HSD1(367N) has limited extragonadal DHT synthesis, whereas 3 β HSD1(367T) augments extragonadal DHT synthesis.¹⁵ The N367T missense is associated with earlier castration resistance and shorter overall survival in multiple clinical studies.^{16,53,54} Therefore, understanding the mechanisms of the adrenal-permissive 3 β HSD1(367T) enzyme is critical to advancing treatment. Here, we show that 3 β HSD1(367T) is degraded via autophagy. Although proteasomal degradation and autophagy were initially considered to act independently of each other, increasing evidence shows their activity to be linked and cooperative.^{10,11} Some proteins have been reported to be degraded by both systems.^{13,14} Our study suggests that 3 β HSD1(367N) and 3 β HSD1(367T) are degraded via different mechanisms. Therefore, the patients with 3 β HSD1(367T) could potentially benefit from autophagy induction.

Interestingly, our results contradict some reports showing that hypoxia can induce autophagy.^{12,55} The major reason for this contradiction may be attributable to the different hypoxic conditions used. Most of these previous studies examined acute hypoxia, whereas we studied chronic hypoxia. Solid tumors commonly contain hypoxic areas due to dynamic gradients of oxygen diffusion, and the cells in hypoxic areas usually experience long-term hypoxia due to inconsistent levels of oxygen and nutrient supply that result from the disorganized tumor vasculature.^{28,56} Prostate tumor is highly hypoxic, and hypoxia plays a critical role in treatment resistance and metastasis.^{19,24,25,27,28,57} Therefore, our HR cell lines, which can survive under hypoxia indefinitely, may better simulate the hypoxic conditions that exist in a tumor.

As the major regulator of the hypoxic response, the HIF family of transcription factors regulates the expression of thousands of genes.^{56,58} Our previous study showed that HIF2 can directly bind the 5' regulatory region of *HSD3B1*.²⁹ However, hypoxia can also regulate various cellular events via HIF-independent mechanisms. Hypoxia has been reported to alter the epigenetic profile of cells, for example, increasing histone methylation and decreasing histone acetylation, and these events occur on both global genomic and gene-specific levels.^{36,37} Hypoxia suppresses the activity of histone demethylase, such as KDM6A, to increase histone methylation.⁵⁹ Compared to HIF, a transcription factor, hypoxia-mediated epigenetic change can more fundamentally alter the gene expression profile and affect a larger number of genes positively or negatively. Our results suggest that chronic hypoxia significantly downregulates ATG expression by reducing histone acetylation. Therefore, in addition to HIF, epigenetic regulators may also be considered as treatment targets in the hypoxic tumor environment.

The diverse roles that autophagy plays in cancer makes it a complex and highly context-dependent therapeutic target.^{12,55,60} Stimulating and suppressing autophagy have both been proposed as cancer therapies. Inhibition of autophagy has been shown to overcome enzalutamide resistance in CRPC.⁶¹ Interestingly, our results here suggest that autophagy decreases androgen synthesis by degrading 3 β HSD1(367T), the enzyme catalyzing the rate-limiting step in androgen synthesis. Consequently, the roles that autophagy plays in tumorigenesis may be context dependent; for example, enzalutamide-resistant CRPC cells may depend less on androgen synthesis for survival, so inhibition of autophagy may not favor the survival of enzalutamide-resistant CRPC cells by increasing the 3 β HSD1 level. That the role of autophagy may depend on context is further supported by a study that shows that autophagy promotes prostate cancer progression in PC3 cells, an AR-negative cell line.⁶² The role of HDACs in regulating autophagy has been reported previously.^{45,63–68} Several HDAC inhibitors have been tested in clinical trials for prostate cancer.^{44–46} However, for various reasons, such as the lack of specificity of the tested inhibitors, the results were not promising. Here, we show a novel mechanism of autophagy regulation by HDACs, specifically that HDACs inhibit ATG transcription. Therefore, our study suggests that HDAC1 may be a better therapeutic target, especially for hypoxic cells, because other HDACs are significantly downregulated under chronic hypoxia.

In summary, our study suggests that chronic hypoxia stabilizes 3 β HSD1(367T) protein by inhibiting its autophagy-mediated degradation. Both ATG mRNA and protein are downregulated under chronic hypoxia. Hypoxia decreases histone acetylation to repress transcription of autophagy regulators. Therefore, HDAC1 may be a therapeutic target for hypoxic prostate cancer cells that are dependent on extragonadal androgen biosynthesis.

Limitations of the study

Although we observed *in vitro* impacts of hypoxia on 3 β HSD1 regulation, we did not determine the parameters of tumor hypoxia or acetylation. Moreover, the extent of tumor hypoxia may largely depend on the volume of tumor. H3K9me2, H3K9ac, and H3K27ac proteins, as representatives of histone modifications, were examined by western blot to determine the overall histone modifications. However, we cannot rule out the possibility that other histone modifications are altered differently from these three. More histone modifications and their links to 3 β HSD1(367T) may need to be examined. Also, acetate is involved in many critical biological events, especially metabolic pathways. Although we treated the cells not only with acetate but also with genetically manipulated *HDAC* and *ACSS* to focus only on the histone acetylation, we still cannot completely exclude other biological processes in which acetate is also involved. Interestingly, HS cells with *ACSS1/2* double knockdown looked normal under normoxia, but HR cells grew more slowly under chronic hypoxia after *ACSS1/2* double knockdown. This suggests that acetate is more critical for HR cell survival under chronic hypoxia than HS cells under normoxia. In Figure 3E, we excluded the outliers to perform a Mann-Whitney test to calculate a two-tailed p value, which was 0.0434.

STAR★METHODS

Detailed methods are provided in the online version of this paper and include the following:

- KEY RESOURCES TABLE
- RESOURCE AVAILABILITY
 - Lead contact
 - Materials availability
 - Data and code availability
- EXPERIMENTAL MODEL AND STUDY PARTICIPANT DETAILS
 - Cell lines
 - Xenograft studies
- METHOD DETAILS
 - qPCR analysis
 - Mass spectrometry
 - Immunoblotting
 - Cell culture
 - Plasmid construction
 - Cell viability assay
 - Global protein synthesis assay
 - LDH sequestration assay
 - LDH enzyme activity assay
 - Mouse xenograft studies
- QUANTIFICATION AND STATISTICAL ANALYSIS

SUPPLEMENTAL INFORMATION

Supplemental information can be found online at <https://doi.org/10.1016/j.celrep.2023.113575>.

ACKNOWLEDGMENTS

We would like to acknowledge Cassandra Talerico, PhD, a salaried employee of the Cleveland Clinic Foundation, for additional editorial comments and review. This work was supported in part by grants from the NCI, NIH (R01CA172382, R01CA236780, R01CA261995, and R01CA249279, to NS; R50CA251961, to MB).

AUTHOR CONTRIBUTIONS

Conceptualization, L.Q., A.A.C., and N.S.; analysis, L.Q., M.B., Y.-M.C., D.C., A.A.C., and N.S.; investigation, L.Q., M.B., Y.-M.C., D.C., and Z.Z.; writing draft, L.Q.; writing – review & editing, L.Q., A.A.C., and N.S.; supervision, N.S.; funding acquisition, L.Q., M.B., and N.S.; methodology, L.Q. and N.S.; project administration, N.S.

DECLARATION OF INTERESTS

N.S. reports grants from BMS and grants from Astellas outside the submitted work; in addition, N.S. has a patent for *HSD3B1* in prostate cancer issued.

Received: June 4, 2023

Revised: October 2, 2023

Accepted: November 28, 2023

Published: January 4, 2024

REFERENCES

1. Siegel, R.L., Miller, K.D., Wagle, N.S., and Jemal, A. (2023). Cancer statistics, 2023. *CA A Cancer J. Clin.* 73, 17–48.
2. Attard, G., Parker, C., Eeles, R.A., Schröder, F., Tomlins, S.A., Tannock, I., Drake, C.G., and de Bono, J.S. (2016). Prostate cancer. *Lancet (London, England)* 387, 70–82.
3. Desai, K., McManus, J.M., and Sharifi, N. (2021). Hormonal Therapy for Prostate Cancer. *Endocr. Rev.* 42, 354–373.
4. Dai, C., Dehm, S.M., and Sharifi, N. (2023). Targeting the Androgen Signaling Axis in Prostate Cancer. *J. Clin. Oncol.* 41, 4267–4278.
5. Wang, G., Zhao, D., Spring, D.J., and DePinho, R.A. (2018). Genetics and biology of prostate cancer. *Genes Dev.* 32, 1105–1140.
6. Sharifi, N. (2013). Minireview: Androgen metabolism in castration-resistant prostate cancer. *Mol. Endocrinol.* 27, 708–714.
7. Michael, P., Roversi, G., Brown, K., and Sharifi, N. (2023). Adrenal Steroids and Resistance to Hormonal Blockade of Prostate and Breast Cancer. *Endocrinology* 164, bqac218.
8. Ferraldeschi, R., Sharifi, N., Auchus, R.J., and Attard, G. (2013). Molecular pathways: Inhibiting steroid biosynthesis in prostate cancer. *Clin. Cancer Res.* 19, 3353–3359.
9. Simard, J., Ricketts, M.L., Gingras, S., Soucy, P., Feltus, F.A., and Melner, M.H. (2005). Molecular biology of the 3 β -hydroxysteroid dehydrogenase/delta5-delta4 isomerase gene family. *Endocr. Rev.* 26, 525–582.
10. Dikic, I. (2017). Proteasomal and Autophagic Degradation Systems. *Annu. Rev. Biochem.* 86, 193–224.
11. Kocaturk, N.M., and Gozuacik, D. (2018). Crosstalk Between Mammalian Autophagy and the Ubiquitin-Proteasome System. *Front. Cell Dev. Biol.* 6, 128.
12. Dikic, I., and Elazar, Z. (2018). Mechanism and medical implications of mammalian autophagy. *Nat. Rev. Mol. Cell Biol.* 19, 349–364.
13. Mitani, T., Minami, M., Harada, N., Ashida, H., and Yamaji, R. (2015). Autophagic degradation of the androgen receptor mediated by increased

- phosphorylation of p62 suppresses apoptosis in hypoxia. *Cell. Signal.* 27, 1994–2001.
14. Liu, X.D., Yao, J., Tripathi, D.N., Ding, Z., Xu, Y., Sun, M., Zhang, J., Bai, S., German, P., Hoang, A., et al. (2015). Autophagy mediates HIF2 α degradation and suppresses renal tumorigenesis. *Oncogene* 34, 2450–2460.
15. Chang, K.H., Li, R., Kuri, B., Lotan, Y., Roehrborn, C.G., Liu, J., Vessella, R., Nelson, P.S., Kapur, P., Guo, X., et al. (2013). A gain-of-function mutation in DHT synthesis in castration-resistant prostate cancer. *Cell* 154, 1074–1084.
16. Thomas, L., and Sharifi, N. (2020). Germline HSD3B1 Genetics and Prostate Cancer Outcomes. *Urology* 145, 13–21.
17. Wicks, E.E., and Semenza, G.L. (2022). Hypoxia-inducible factors: cancer progression and clinical translation. *J. Clin. Invest.* 132, e159839.
18. Lee, P., Chandel, N.S., and Simon, M.C. (2020). Cellular adaptation to hypoxia through hypoxia inducible factors and beyond. *Nat. Rev. Mol. Cell Biol.* 21, 268–283.
19. Jans, J., van Dijk, J.H., van Schelven, S., van der Groep, P., Willems, S.H., Jonges, T.N., van Diest, P.J., and Bosch, J.L.H.R. (2010). Expression and localization of hypoxia proteins in prostate cancer: prognostic implications after radical prostatectomy. *Urology* 75, 786–792.
20. Tong, D., Liu, Q., Liu, G., Yuan, W., Wang, L., Guo, Y., Lan, W., Zhang, D., Dong, S., Wang, Y., et al. (2016). The HIF/PHF8/AR axis promotes prostate cancer progression. *Oncogenesis* 5, e283.
21. Khandrika, L., Lieberman, R., Koul, S., Kumar, B., Maroni, P., Chandhoke, R., Meacham, R.B., and Koul, H.K. (2009). Hypoxia-associated p38 mitogen-activated protein kinase-mediated androgen receptor activation and increased HIF-1 α levels contribute to emergence of an aggressive phenotype in prostate cancer. *Oncogene* 28, 1248–1260.
22. Ranasinghe, W.K.B., Baldwin, G.S., Bolton, D., Shulkes, A., Ischia, J., and Patel, O. (2015). HIF1 α expression under normoxia in prostate cancer— which pathways to target? *J. Urol.* 193, 763–770.
23. Mitani, T., Yamaji, R., Higashimura, Y., Harada, N., Nakano, Y., and Inui, H. (2011). Hypoxia enhances transcriptional activity of androgen receptor through hypoxia-inducible factor-1 α in a low androgen environment. *J. Steroid Biochem. Mol. Biol.* 123, 58–64.
24. Deep, G., and Panigrahi, G.K. (2015). Hypoxia-Induced Signaling Promotes Prostate Cancer Progression: Exosomes Role as Messenger of Hypoxic Response in Tumor Microenvironment. *Crit. Rev. Oncog.* 20, 419–434.
25. Fraga, A., Ribeiro, R., Príncipe, P., Lopes, C., and Medeiros, R. (2015). Hypoxia and Prostate Cancer Aggressiveness: A Tale With Many Endings. *Clin. Genitourin. Cancer* 13, 295–301.
26. Ashton, J., and Bristow, R. (2020). Bad neighbours: hypoxia and genomic instability in prostate cancer. *Br. J. Radiol.* 93, 20200087.
27. Ragnum, H.B., Vlatkovic, L., Lie, A.K., Axcrone, K., Julin, C.H., Friestad, K.M., Hole, K.H., Seierstad, T., and Lyng, H. (2015). The tumour hypoxia marker pimonidazole reflects a transcriptional programme associated with aggressive prostate cancer. *Br. J. Cancer* 112, 382–390.
28. Bhandari, V., Hoey, C., Liu, L.Y., Lalonde, E., Ray, J., Livingstone, J., Lesurf, R., Shiah, Y.J., Vujcic, T., Huang, X., et al. (2019). Molecular landmarks of tumor hypoxia across cancer types. *Nat. Genet.* 51, 308–318.
29. Qin, L., Chung, Y.M., Berk, M., Naelitz, B., Zhu, Z., Klein, E., Chakraborty, A.A., and Sharifi, N. (2022). Hypoxia-Reoxygenation Couples 3 β HSD1 Enzyme and Cofactor Upregulation to Facilitate Androgen Biosynthesis and Hormone Therapy Resistance in Prostate Cancer. *Cancer Res.* 82, 2417–2430.
30. Dowdle, W.E., Nyfeler, B., Nagel, J., Elling, R.A., Liu, S., Triantafellow, E., Menon, S., Wang, Z., Honda, A., Pardee, G., et al. (2014). Selective VPS34 inhibitor blocks autophagy and uncovers a role for NCOA4 in ferritin degradation and iron homeostasis in vivo. *Nat. Cell Biol.* 16, 1069–1079.
31. Petherick, K.J., Conway, O.J.L., Mpamhanga, C., Osborne, S.A., Kamal, A., Saxty, B., and Ganley, I.G. (2015). Pharmacological inhibition of ULK1 kinase blocks mammalian target of rapamycin (mTOR)-dependent autophagy. *J. Biol. Chem.* 290, 11376–11383.
32. Martin, K.R., Celano, S.L., Solitro, A.R., Gunaydin, H., Scott, M., O'Hagan, R.C., Shumway, S.D., Fuller, P., and MacKeigan, J.P. (2018). A Potent and Selective ULK1 Inhibitor Suppresses Autophagy and Sensitizes Cancer Cells to Nutrient Stress. *iScience* 8, 74–84.
33. Kaushik, S., and Cuervo, A.M. (2018). The coming of age of chaperone-mediated autophagy. *Nat. Rev. Mol. Cell Biol.* 19, 365–381.
34. Chee, N.T., Lohse, I., and Brothers, S.P. (2019). mRNA-to-protein translation in hypoxia. *Mol. Cancer* 18, 49.
35. Xia, X., and Kung, A.L. (2009). Preferential binding of HIF-1 to transcriptionally active loci determines cell-type specific response to hypoxia. *Genome Biol.* 10, R113.
36. Kim, J., Lee, H., Yi, S.J., and Kim, K. (2022). Gene regulation by histone-modifying enzymes under hypoxic conditions: a focus on histone methylation and acetylation. *Exp. Mol. Med.* 54, 878–889.
37. Kim, I., and Park, J.W. (2020). Hypoxia-driven epigenetic regulation in cancer progression: A focus on histone methylation and its modifying enzymes. *Cancer Lett.* 489, 41–49.
38. Dawson, M.A. (2017). The cancer epigenome: Concepts, challenges, and therapeutic opportunities. *Science* 355, 1147–1152.
39. Baratchian, M., Tiwari, R., Khalighi, S., Chakravarthy, A., Yuan, W., Berk, M., Li, J., Gueriot, A., de Bono, J., Makarov, V., et al. (2022). H3K9 methylation drives resistance to androgen receptor-antagonist therapy in prostate cancer. *Proc. Natl. Acad. Sci. USA* 119, e2114324119.
40. Liu, F., Barsyte-Lovejoy, D., Li, F., Xiong, Y., Korboukh, V., Huang, X.P., Allali-Hassani, A., Janzen, W.P., Roth, B.L., Frye, S.V., et al. (2013). Discovery of an in vivo chemical probe of the lysine methyltransferases G9a and GLP. *J. Med. Chem.* 56, 8931–8942.
41. Sweis, R.F., Pliushchev, M., Brown, P.J., Guo, J., Li, F., Maag, D., Petros, A.M., Soni, N.B., Tse, C., Vedadi, M., et al. (2014). Discovery and development of potent and selective inhibitors of histone methyltransferase g9a. *ACS Med. Chem. Lett.* 5, 205–209.
42. Richon, V.M., Emiliani, S., Verdin, E., Webb, Y., Breslow, R., Rifkind, R.A., and Marks, P.A. (1998). A class of hybrid polar inducers of transformed cell differentiation inhibits histone deacetylases. *Proc. Natl. Acad. Sci. USA* 95, 3003–3007.
43. Davie, J.R. (2003). Inhibition of histone deacetylase activity by butyrate. *J. Nutr.* 133, 2485s–2493s.
44. Rana, Z., Diermeier, S., Hanif, M., and Rosengren, R.J. (2020). Understanding Failure and Improving Treatment Using HDAC Inhibitors for Prostate Cancer. *Biomedicines* 8, 22.
45. Koeneke, E., Witt, O., and Oehme, I. (2015). HDAC Family Members Intertwined in the Regulation of Autophagy: A Druggable Vulnerability in Aggressive Tumor Entities. *Cells* 4, 135–168.
46. Biersack, B., Nitzsche, B., and Höpfner, M. (2022). HDAC inhibitors with potential to overcome drug resistance in castration-resistant prostate cancer. *Cancer Drug Resist.* 5, 64–79.
47. Li, Y., Gruber, J.J., Litzenburger, U.M., Zhou, Y., Miao, Y.R., LaGory, E.L., Li, A.M., Hu, Z., Yip, M., Hart, L.S., et al. (2020). Acetate supplementation restores chromatin accessibility and promotes tumor cell differentiation under hypoxia. *Cell Death Dis.* 11, 102.
48. Gao, X., Lin, S.H., Ren, F., Li, J.T., Chen, J.J., Yao, C.B., Yang, H.B., Jiang, S.X., Yan, G.Q., Wang, D., et al. (2016). Acetate functions as an epigenetic metabolite to promote lipid synthesis under hypoxia. *Nat. Commun.* 7, 11960.
49. Guertin, D.A., and Wellen, K.E. (2023). Acetyl-CoA metabolism in cancer. *Nat. Rev. Cancer* 23, 156–172.
50. Dai, C., Chung, Y.M., Kovac, E., Zhu, Z., Li, J., Magi-Galluzzi, C., Stephenson, A.J., Klein, E.A., and Sharifi, N. (2017). Direct Metabolic Interrogation of Dihydrotestosterone Biosynthesis from Adrenal Precursors in Primary Prostatectomy Tissues. *Clin. Cancer Res.* 23, 6351–6362.

51. Li, X., Berk, M., Goins, C., Alyamani, M., Chung, Y.M., Wang, C., Patel, M., Rath, N., Zhu, Z., Willard, B., et al. (2023). BMX controls 3 β HSD1 and sex steroid biosynthesis in cancer. *J. Clin. Invest.* 133, e163498.
52. Cui, D., Li, J., Zhu, Z., Berk, M., Hardaway, A., McManus, J., Chung, Y.M., Alyamani, M., Valle, S., Tiwari, R., et al. (2023). Cancer-associated fibroblast-secreted glucosamine alters the androgen biosynthesis program in prostate cancer via HSD3B1 upregulation. *J. Clin. Invest.* 133, e161913.
53. Hearn, J.W.D., Sweeney, C.J., Almassi, N., Reichard, C.A., Reddy, C.A., Li, H., Hobbs, B., Jarrard, D.F., Chen, Y.H., Dreicer, R., et al. (2020). HSD3B1 Genotype and Clinical Outcomes in Metastatic Castration-Sensitive Prostate Cancer. *JAMA Oncol.* 6, e196496.
54. Hearn, J.W.D., Xie, W., Nakabayashi, M., Almassi, N., Reichard, C.A., Pomerantz, M., Kantoff, P.W., and Sharifi, N. (2018). Association of HSD3B1 Genotype With Response to Androgen-Deprivation Therapy for Biochemical Recurrence After Radiotherapy for Localized Prostate Cancer. *JAMA Oncol.* 4, 558–562.
55. Levy, J.M.M., Towers, C.G., and Thorburn, A. (2017). Targeting autophagy in cancer. *Nat. Rev. Cancer* 17, 528–542.
56. Wigerup, C., Pahlman, S., and Bexell, D. (2016). Therapeutic targeting of hypoxia and hypoxia-inducible factors in cancer. *Pharmacol. Ther.* 164, 152–169.
57. Mohamed, O.A.A., Tesen, H.S., Hany, M., Sherif, A., Abdelwahab, M.M., and Elnaggar, M.H. (2023). The role of hypoxia on prostate cancer progression and metastasis. *Mol. Biol. Rep.* 50, 3873–3884.
58. Wilkins, S.E., Abboud, M.I., Hancock, R.L., and Schofield, C.J. (2016). Targeting Protein-Protein Interactions in the HIF System. *ChemMedChem* 11, 773–786.
59. Chakraborty, A.A., Laukka, T., Myllykoski, M., Ringel, A.E., Booker, M.A., Tolstorukov, M.Y., Meng, Y.J., Meier, S.R., Jennings, R.B., Creech, A.L., et al. (2019). Histone demethylase KDM6A directly senses oxygen to control chromatin and cell fate. *Science* 363, 1217–1222.
60. Amaravadi, R.K., Kimmelman, A.C., and Debnath, J. (2019). Targeting Autophagy in Cancer: Recent Advances and Future Directions. *Cancer Discov.* 9, 1167–1181.
61. Nguyen, H.G., Yang, J.C., Kung, H.J., Shi, X.B., Tilki, D., Lara, P.N., Jr., De Vere White, R.W., Gao, A.C., and Evans, C.P. (2014). Targeting autophagy overcomes Enzalutamide resistance in castration-resistant prostate cancer cells and improves therapeutic response in a xenograft model. *Oncogene* 33, 4521–4530.
62. Yu, K., Xiang, L., Li, S., Wang, S., Chen, C., and Mu, H. (2019). HIF1 α promotes prostate cancer progression by increasing ATG5 expression. *Anim. Cell Syst.* 23, 326–334.
63. Körholz, K., Ridinger, J., Kronic, D., Najafi, S., Gerloff, X.F., Frese, K., Meder, B., Peterziel, H., Vega-Rubin-de-Celis, S., Witt, O., and Oehme, I. (2021). Broad-Spectrum HDAC Inhibitors Promote Autophagy through FOXO Transcription Factors in Neuroblastoma. *Cells* 10.
64. Yang, J., He, J., Ismail, M., Tweeken, S., Zeng, F., Gao, L., Ballinger, S., Young, M., Prabhu, S.D., Rowe, G.C., et al. (2019). HDAC inhibition induces autophagy and mitochondrial biogenesis to maintain mitochondrial homeostasis during cardiac ischemia/reperfusion injury. *J. Mol. Cell. Cardiol.* 130, 36–48.
65. Shi, L., Song, Z., Li, C., Deng, F., Xia, Y., Huang, J., Wu, X., and Zhu, J. (2022). HDAC6 Inhibition Alleviates Ischemia- and Cisplatin-Induced Acute Kidney Injury by Promoting Autophagy. *Cells* 11.
66. Chiu, C.F., Chin, H.K., Huang, W.J., Bai, L.Y., Huang, H.Y., and Weng, J.R. (2019). Induction of Apoptosis and Autophagy in Breast Cancer Cells by a Novel HDAC8 Inhibitor. *Biomolecules* 9, 824.
67. Zeyen, P., Zeyn, Y., Herp, D., Mahmoudi, F., Yesiloglu, T.Z., Erdmann, F., Schmidt, M., Robaa, D., Romier, C., Ridinger, J., et al. (2022). Identification of histone deacetylase 10 (HDAC10) inhibitors that modulate autophagy in transformed cells. *Eur. J. Med. Chem.* 234, 114272.
68. Ge, W., Luo, S., Zhang, K., Liu, L., Zhou, Z., and Liu, Y. (2023). Role of histone deacetylase 9 in human periodontal ligament stem cells autophagy in a tumour necrosis factor α -induced inflammatory environment. *Tissue Cell* 82, 102113.
69. Sanjana, N.E., Shalem, O., and Zhang, F. (2014). Improved vectors and genome-wide libraries for CRISPR screening. *Nat. Methods* 11, 783–784.
70. Luhr, M., Szalai, P., and Engedal, N. (2018). The Lactate Dehydrogenase Sequestration Assay - A Simple and Reliable Method to Determine Bulk Autophagic Sequestration Activity in Mammalian Cells. *J. Vis. Exp.*, 57971.

STAR★METHODS

KEY RESOURCES TABLE

REAGENT or RESOURCE	SOURCE	IDENTIFIER
Antibodies		
Mouse monoclonal anti-HDAC10	Santa Cruz Biotechnology	sc-393714
Mouse monoclonal anti-HDAC11	Santa Cruz Biotechnology	sc-390737;RRID:AB_2715508
Mouse monoclonal anti- β -actin	Sigma-Aldrich	A2228;RRID:AB_476697
Mouse monoclonal anti-FLAG-Tag	Sigma-Aldrich	F1804;RRID:AB_262044
Rabbit polyclonal anti-HSPA8	Proteintech Group	10654-1-AP;RRID:AB_2120153
Rabbit polyclonal anti-LAMP2	Proteintech Group	27823-1-AP;RRID:AB_2880983
Rabbit polyclonal anti-ACSS1	Proteintech Group	17138-1-AP;RRID:AB_2289182
Rabbit monoclonal anti-ATG10	Abcam	ab124711;RRID:AB_10974774
Mouse monoclonal anti- β HSD1	Abcam	ab55268;RRID:AB_942015
Rabbit monoclonal anti-HDAC8	Abcam	ab187139;RRID:AB_2715505
Rabbit monoclonal anti-HDAC9	Abcam	ab109446;RRID:AB_10861804
Rabbit polyclonal anti-Histone H3	Abcam	ab1791;RRID:AB_302613
Rabbit polyclonal anti-P62	Cell Signaling	5114;RRID:AB_10624872
Rabbit monoclonal anti-HA-Tag	Cell Signaling	3724;RRID:AB_1549585
Rabbit monoclonal anti-ULK1	Cell Signaling	8054;RRID:AB_11178668
Rabbit polyclonal anti-ATG2A	Cell Signaling	15011;RRID:AB_2732797
Rabbit polyclonal anti-ATG3	Cell Signaling	3415;RRID:AB_2059244
Rabbit monoclonal anti-ATG4A	Cell Signaling	7613;RRID:AB_10827645
Rabbit monoclonal anti-ATG4B	Cell Signaling	13507;RRID:AB_2750642
Rabbit monoclonal anti-ATG5	Cell Signaling	12994;RRID:AB_2630393
Rabbit monoclonal anti-Becclin-1	Cell Signaling	3495;RRID:AB_1903911
Rabbit monoclonal anti-ATG7	Cell Signaling	8558;RRID:AB_10831194
Rabbit monoclonal anti-LC3A	Cell Signaling	4599;RRID:AB_10548192
Rabbit polyclonal anti-LC3B	Cell Signaling	2775;RRID:AB_915950
Rabbit monoclonal anti-GABARAP	Cell Signaling	13733;RRID:AB_2798306
Rabbit monoclonal anti-ATG9A	Cell Signaling	13509;RRID:AB_2798241
Rabbit monoclonal anti-ATG12	Cell Signaling	4180;RRID:AB_1903898
Rabbit polyclonal anti-ATG14	Cell Signaling	5504;RRID:AB_10695397
Rabbit monoclonal anti-ATG16L1	Cell Signaling	8089;RRID:AB_10950320
Rabbit polyclonal anti-WIP1	Cell Signaling	12124;RRID:AB_2750868
Rabbit polyclonal anti-WIP2	Cell Signaling	8567;RRID:AB_11178945
Mouse monoclonal anti-Myc-Tag	Cell Signaling	2276;RRID:AB_331783
Rabbit monoclonal anti-HDAC1	Cell Signaling	34589;RRID:AB_2756821
Rabbit monoclonal anti-HDAC2	Cell Signaling	57156;RRID:AB_2756828
Rabbit monoclonal anti-HDAC3	Cell Signaling	85057;RRID:AB_2800047
Rabbit monoclonal anti-HDAC4	Cell Signaling	15164;RRID:AB_2798733
Rabbit monoclonal anti-HDAC5	Cell Signaling	20458;RRID:AB_2713973
Rabbit monoclonal anti-HDAC6	Cell Signaling	7612;RRID:AB_10889735
Rabbit monoclonal anti-HDAC7	Cell Signaling	33418;RRID:AB_2716756
Rabbit monoclonal anti-Di-Methyl-Histone H3 (Lys9)	Cell Signaling	4658;RRID:AB_10544405
Rabbit monoclonal anti-Acetyl-Histone H3 (Lys9)	Cell Signaling	9649;RRID:AB_823528
Rabbit monoclonal anti-Acetyl-Histone H3 (Lys27)	Cell Signaling	8173;RRID:AB_10949503
Rabbit monoclonal anti-ACSS2	Cell Signaling	3658;RRID:AB_2222710

(Continued on next page)

Continued

REAGENT or RESOURCE	SOURCE	IDENTIFIER
Goat anti-rabbit IgG	Cell Signaling	7074;RRID:AB_2099233
Horse anti-mouse IgG	Cell Signaling	7076;RRID:AB_330924
Chemicals, peptides, and recombinant proteins		
Lipofectamine 3000 Transfection Reagent	Thermo Fisher Scientific	L3000015
Lipofectamine RNAiMAX Transfection Reagent	Thermo Fisher Scientific	13778075
sodium butyrate	Sigma-Aldrich	B5887
dimethyl sulfoxide (DMSO)	Sigma-Aldrich	D2650
acetate solution	Sigma-Aldrich	3863
3-methyladenine	Sigma-Aldrich	M9281
chloroquine diphosphate salt	Sigma-Aldrich	C6628
Puromycin	Gibco	A1113803
penicillin streptomycin	Gibco	15140122
L-Glutamine 200mM	Gibco	25030081
Tat-beclin 1 (Tat-BECN1)	Selleck Chemicals	S8595
MG132	Selleck Chemicals	S2619
Rapamycin	Selleck Chemicals	S1039
ULK-101	Selleck Chemicals	S8793
MRT68921 HCl	Selleck Chemicals	S7949
PIK-III	Selleck Chemicals	S7683
UNC0642	Selleck Chemicals	S7230
A-366	Selleck Chemicals	S7572
vorinostat (SAHA)	Selleck Chemicals	S1047
panobinostat (LBH589)	Selleck Chemicals	S1030
belinostat (PXD101)	Selleck Chemicals	S1085
bafilomycin A1	MedChemExpress	HY-100558
Critical commercial assays		
QuikChange Lightning Multi Site-Directed Mutagenesis Kit	Agilent Technologies	210515
CellTiter-Glo 2.0 Cell Viability Assay	Promega	G9241
Global Protein Synthesis Assay Kit	Abcam	ab273286
Experimental models: Cell lines		
LNCaP cell line	ATCC	N/A
C4-2 cell line	Dr. Leland Chung (Cedars-Sinai Medical Center, CA)	N/A
LAPC4 cell line	Dr. Charles Sawyers (Memorial Sloan Kettering Cancer, NY).	N/A
Experimental models: Organisms/strains		
Male NSG mice (6–8 weeks old) for xenografts of human prostate cancer cell lines	Cleveland Clinic Lerner Research Institute	N/A
Oligonucleotides		
<i>HSD3B1</i> qPCR Forward: GATTCCAGATGGAGCTTTCCT	Integrated DNA Technologies	N/A
<i>HSD3B1</i> qPCR Reverse: GGCGGTTCGATAGGTGTAAAT	Integrated DNA Technologies	N/A
<i>ACTB</i> qPCR Forward: ACCTTCTACAATGAGCTGCG	Integrated DNA Technologies	N/A
<i>ACTB</i> qPCR Reverse: CCTGGATAGCAACGTACATGG	Integrated DNA Technologies	N/A
<i>ULK1</i> qPCR Forward: TGGGCAAGTTCGAGTTCTC	Integrated DNA Technologies	N/A
<i>ULK1</i> qPCR Reverse: CTTGTTAATGCACCTTGACGGC	Integrated DNA Technologies	N/A
<i>ATG2A</i> qPCR Forward: TGGAGCTGATGGTGAAGTTG	Integrated DNA Technologies	N/A

(Continued on next page)

Continued

REAGENT or RESOURCE	SOURCE	IDENTIFIER
ATG2A qPCR Reverse: AGTTCCTGAAGTTGCTGGAG	Integrated DNA Technologies	N/A
ATG3 qPCR Forward: GGCGGTGAAGATGCTATTTTG	Integrated DNA Technologies	N/A
ATG3 qPCR Reverse: GTGCTCAACTGTTAAAGGCTG	Integrated DNA Technologies	N/A
ATG4A qPCR Forward: ACACTGAAGAGAATGGAACGG	Integrated DNA Technologies	N/A
ATG4A qPCR Reverse: CAAGGCTACACCAGTTATCAAAG	Integrated DNA Technologies	N/A
ATG4B qPCR Forward: GTGGCATCTAGACTTTGGTTTAC	Integrated DNA Technologies	N/A
ATG4B qPCR Reverse: AGGGCTTGGGCAAAGATC	Integrated DNA Technologies	N/A
ATG5 qPCR Forward: TGTTTCGCTCTGTGGCTG	Integrated DNA Technologies	N/A
ATG5 qPCR Reverse: GCAGAGGTGTTTCCAACATTG	Integrated DNA Technologies	N/A
BECN1 qPCR Forward: CGTCTTTAATGCAACCTTCCAC	Integrated DNA Technologies	N/A
BECN1 qPCR Reverse: CGACCCAGCCTGAAGTTATTG	Integrated DNA Technologies	N/A
ATG7 qPCR Forward: AAACAGAAGGAGTCACAGCTC	Integrated DNA Technologies	N/A
ATG7 qPCR Reverse: GGGCTAAGTTACAGGGATCATATAC	Integrated DNA Technologies	N/A
LC3A qPCR Forward: ACCCCAGCAAAATCCCG	Integrated DNA Technologies	N/A
LC3A qPCR Reverse: TCTTGACCAACTCGCTCATG	Integrated DNA Technologies	N/A
LC3B qPCR Forward: AAGTTCCTGTACCTGACCATG	Integrated DNA Technologies	N/A
LC3B qPCR Reverse: CTGAGATTGGTGTGGAGACG	Integrated DNA Technologies	N/A
GABARAP qPCR Forward: AAGAGCATCCGTTGAGAAG	Integrated DNA Technologies	N/A
GABARAP qPCR Reverse: TCAGAAGGCACCAGGTATTTTC	Integrated DNA Technologies	N/A
ATG9A qPCR Forward: AGATGTGTTGGCTGTGGAAC	Integrated DNA Technologies	N/A
ATG9A qPCR Reverse: CATGTAGTGGATGTGAGCGAG	Integrated DNA Technologies	N/A
ATG10 qPCR Forward: TCAAAGGACTGTTCTGATGGC	Integrated DNA Technologies	N/A
ATG10 qPCR Reverse: CATCCAAGGGTAGCTCGAAAG	Integrated DNA Technologies	N/A
ATG12 qPCR Forward: ACCATCCAAGGACTCATTGAC	Integrated DNA Technologies	N/A
ATG12 qPCR Reverse: CCATCACTGCCAAAACACTC	Integrated DNA Technologies	N/A
ATG13 qPCR Forward: AGCAATCAAAGACATCCCAGAG	Integrated DNA Technologies	N/A
ATG13 qPCR Reverse: AGACACCATATTTCCAGCTCC	Integrated DNA Technologies	N/A
ATG14 qPCR Forward: GGAAGTAAAGACGGGTGTGAG	Integrated DNA Technologies	N/A
ATG14 qPCR Reverse: GTGTCTCCGTTGTGATCGTC	Integrated DNA Technologies	N/A
ATG16L1 qPCR Forward: CCGAATCTGGACTGTGGATG	Integrated DNA Technologies	N/A
ATG16L1 qPCR Reverse: GCGTAGATCCCAGAGTTTGAG	Integrated DNA Technologies	N/A
WIPI1 qPCR Forward: ACGGTGCCAGGTTATTCTG	Integrated DNA Technologies	N/A
WIPI1 qPCR Reverse: CGTTTTGCCCTTCTGATTTC	Integrated DNA Technologies	N/A
WIPI2 qPCR Forward: ACAGTCCTTTAGCGGCAC	Integrated DNA Technologies	N/A
WIPI2 qPCR Reverse: CTCACGCACCTCTTTACTCC	Integrated DNA Technologies	N/A
KLK3 qPCR Forward: AGAGCTGTGTACCATGTG	Integrated DNA Technologies	N/A
KLK3 qPCR Reverse: AGGGTTGGGAATGCTTCTC	Integrated DNA Technologies	N/A
FKBP5 qPCR Forward: CAGTCTCCCTAAATTCCTCG	Integrated DNA Technologies	N/A
FKBP5 qPCR Reverse: TTGCTCCTTCGTTTGATTTC	Integrated DNA Technologies	N/A
TMPRSS2 qPCR Forward: GGAGTGTACGGGAATGTGATG	Integrated DNA Technologies	N/A
TMPRSS2 qPCR Reverse: CCAGCCCCATTGTTTCTTG	Integrated DNA Technologies	N/A
ACSS1 qPCR Forward: TTGAGAGCACCCAGTTTATC	Integrated DNA Technologies	N/A
ACSS1 qPCR Reverse: GCATCACCGTATTTTACGCAAC	Integrated DNA Technologies	N/A
ACSS2 qPCR Forward: GGGAAGAGTTGGAAGGTGAAG	Integrated DNA Technologies	N/A
ACSS2 qPCR Reverse: GCAGCCATCTCTGTAAACATAG	Integrated DNA Technologies	N/A
HDAC1 qPCR Forward: CGGTGCTGGACATATGAGAC	Integrated DNA Technologies	N/A
HDAC1 qPCR Reverse: ATATTGGAAGGACTGATGTGGAG	Integrated DNA Technologies	N/A

(Continued on next page)

Continued

REAGENT or RESOURCE	SOURCE	IDENTIFIER
HDAC2 qPCR Forward: TGACAAACCAGAACTCCAG	Integrated DNA Technologies	N/A
HDAC2 qPCR Reverse: CTTCTCCATCTTCATCTCCACTG	Integrated DNA Technologies	N/A
HDAC3 qPCR Forward: GGACTTCTACCAACCCACG	Integrated DNA Technologies	N/A
HDAC3 qPCR Reverse: CAGCACGAGTAGAGGGATATTG	Integrated DNA Technologies	N/A
HDAC4 qPCR Forward: CATGTGTTTCTGCCTTGCTG	Integrated DNA Technologies	N/A
HDAC4 qPCR Reverse: CAGTACTTGCTGTGGATCTCC	Integrated DNA Technologies	N/A
HDAC5 qPCR Forward: TCACCGCAAACTCCTACAG	Integrated DNA Technologies	N/A
HDAC5 qPCR Reverse: AGTTCCCGTTGTCATAGCG	Integrated DNA Technologies	N/A
HDAC6 qPCR Forward: TGAATTCCATTGCCTCTGGG	Integrated DNA Technologies	N/A
HDAC6 qPCR Reverse: TGAACCAACATCAGCTCTTCC	Integrated DNA Technologies	N/A
HDAC7 qPCR Forward: GATAGTCGTGATGCCCATCG	Integrated DNA Technologies	N/A
HDAC7 qPCR Reverse: GCTGCGTCATGTATCCAAAC	Integrated DNA Technologies	N/A
HDAC8 qPCR Forward: ACCTCCACACTGATGCTTATC	Integrated DNA Technologies	N/A
HDAC8 qPCR Reverse: AGTCAAATATCCCTTCAGTGGC	Integrated DNA Technologies	N/A
HDAC9 qPCR Forward: AGCCACCTCATGTTACTTTAG	Integrated DNA Technologies	N/A
HDAC9 qPCR Reverse: AGGGAGACTGAGGATGTAAGG	Integrated DNA Technologies	N/A
HDAC10 qPCR Forward: TCACATTGGTTCTGCCCC	Integrated DNA Technologies	N/A
HDAC10 qPCR Reverse: TCCCATCTAAGAGGTACAGGAG	Integrated DNA Technologies	N/A
HDAC11 qPCR Forward: GTTCTGTTTGAGCGTGTGG	Integrated DNA Technologies	N/A
HDAC11 qPCR Reverse: GGTAGATGTGGCGTTGTAG	Integrated DNA Technologies	N/A
HSPA8 siRNA sequence: GAGUUUAAGCGCAAGCAUAtt/ UAUGCUUGCGCUAAACUCag	Thermo Fisher Scientific	s6985
siRNA negative control	Thermo Fisher Scientific	4390846
Recombinant DNA		
BECN1 shRNA sequence: CCGGCCCGTGGAATGGAATGAGATTCTCGAGAATCTC ATTCCATTCCACGGGTTTTTG	Sigma-Aldrich	TRCN0000033549
ATG5 shRNA sequence: CCGGCCTGAACAGAATCATCTTAACGAGTTAAGG ATGATTCTGTTCCAGGTTTTTG	Sigma-Aldrich	TRCN0000151963
LAMP2 shRNA mature antisense: TGTCGTCATCTGCACTGCA	Horizon Discovery	RHS4430-200266529
HDAC1 shRNA targeting sequence: CGGTTAGGTTGC TTCAATCTA	Sigma-Aldrich	TRCN0000195467
ACSS1 shRNA targeting sequence: CTGTTGCTGAAA TACGGTGAT	Sigma-Aldrich	TRCN0000045380
ACSS2 shRNA targeting sequence: GCTTGAGATAA AGTTGCTTT	Sigma-Aldrich	TRCN0000045564
Negative control shRNA (Horizon Discovery)	Horizon Discovery	RHS4346
Negative control shRNA (Sigma-Aldrich) targeting sequence: CCGGCAACAAGATGAAGAGCACCAACTCGA GTTGGTGCTTTCATCTTGTGTTTTT	Sigma-Aldrich	SHC002
Plasmid pCMV3-OFPSpark-LC3A expressing N-terminal OFPSpark-tagged LC3A	Sino Biological	HG14322-ANR
Plasmid pCMV3-HSD3B1-HA expressing C-terminal HA tagged HSD3B1	Sino Biological	HG14410-CY
Plasmid pCMV3-HSPA8-Myc expressing C-terminal Myc tagged HSPA8	Sino Biological	HG11329-CM
Plasmid pCMV3-ACSS1 expressing ACSS1	Sino Biological	HG12250-UT

(Continued on next page)

Continued

REAGENT or RESOURCE	SOURCE	IDENTIFIER
Plasmid pCMV3-ACSS2-HA expressing C-terminal HA tagged ACSS2	Sino Biological	HG22964-CY
Plasmid pcDNA3.1+-LAMP2-(K)DYK expressing C-terminal Flag-tagged LAMP2 (transcript variant A)	GenScript	OHu23655D
Plasmid pCMV3-HSD3B1(1245C)-HA expressing C-terminal HA-tagged HSD3B1(1245C)	This study	N/A
Software and algorithms		
ImageJ	https://ImageJ.nih.gov/ij/	N/A

RESOURCE AVAILABILITY

Lead contact

Further information and requests for resources and reagents should be directed to and will be fulfilled by the lead contact, Nima Sharifi (nxs1664@miami.edu).

Materials availability

This study did not generate new unique reagents.

Data and code availability

- Original data are available from the [lead contact](#) up on request.
- This paper does not report original code.
- Any additional information required to reanalyze the data reported in this paper is available from the [lead contact](#) up on request.

EXPERIMENTAL MODEL AND STUDY PARTICIPANT DETAILS

Cell lines

The LNCaP cell line was purchased from ATCC. The C4-2 cell line was generously provided by Dr. Leland Chung (Cedars-Sinai Medical Center, CA). The LAPC4 cell line was generously provided by Dr. Charles Sawyers (Memorial Sloan Kettering Cancer, NY).

Xenograft studies

Male NSG mice (6–8 weeks old) were purchased from the Cleveland Clinic Lerner Research Institute. All mouse studies were performed under a protocol approved by the Institutional animal care and use committee of the Cleveland Clinic.

METHOD DETAILS

qPCR analysis

Total RNA was extracted using the GenElute Mammalian Total RNA Miniprep Kit (RTN350-1KT) from Sigma-Aldrich. Total RNA, 2 μ g, was used to synthesize cDNA in a reverse-transcriptase reaction with the iScript cDNA Synthesis Kit (170–8891) from Bio-Rad. Primers, cDNA, and iTaq Universal SYBR Green Supermix (1725124) from Bio-Rad were mixed and then loaded in a real-time PCR instrument (ABI-7500) from Applied Biosystems to perform qPCR. The sample values were normalized to *ACTB* and then to the control samples to quantify the mRNA. The qPCR results are shown as the mean values of three independent experiments.

Mass spectrometry

For medium samples, 200 μ L medium from steroid-treated cell culture was mixed with 200 μ L H₂O, 2 mL methyl *tert*-butyl ether, and 10 μ L [2, 3, 4-¹³C₃] AD (50 ng/mL) as internal standard and then vortexed for 10 min. The mixture was centrifuged at 3000g for 5 min at 4°C and then placed on dry ice for 5 min to freeze the bottom layer. The top organic layer with the steroid was transferred to a new glass tube and then evaporated with nitrogen gas at 40°C. The dry steroid was reconstituted in 120 μ L 50% methanol and then vortexed for 5 min. The sample was centrifuged at 3000g for 3 min at 4°C and then transferred into a 1.5 mL microcentrifuge tube. After centrifugation at 14000g for 10 min at 4°C, 90 μ L supernatant was collected in an HPLC vial for mass spectrometry. For xenograft tumor sample, the weighed sample (>30 mg) was transferred to tubes (MK28) from Bertin Technologies for grinding hard tissues and then snap-frozen in liquid nitrogen. The tissue was suspended in 900 μ L cold acetonitrile with 10 μ L [2, 3, 4-¹³C₃] AD (50 ng/mL) as primary internal standard and then homogenized using a Minilys homogenizer at 4°C. After centrifugation at 14000g for 10 min at 4°C, the supernatant was

transferred into a new glass tube and then mixed with 500 μ L cold H₂O. The mixture was vortexed for 2 min and then centrifuged at 14000g for 10 min at 4°C. The supernatant was transferred and combined with the supernatant from the previous steps, as well as 10 μ L DHT-d3 (25 ng/mL) as a secondary internal standard. The steroids were extracted following the protocol for media samples described above.

Immunoblotting

Cells were lysed with loading buffer (2% SDS, 10% glycerol, 10 mM Tris, pH6.8, 100 mM DTT) and then boiled for 10 min to extract protein. The samples were loaded on an SDS-PAGE gel using a standard Tris-glycine buffer system, and then transferred to a PVDF membrane. The membrane was incubated in TBST (137 mM NaCl, 20 mM Tris, 0.1% Tween 20, pH7.6) containing 5% non-fat dry milk for 1 h at room temperature, and then with primary antibody at the appropriate dilution (see [key resources table](#)) at 4°C overnight. The membrane was washed with TBST and then incubated with secondary antibody at 1:10000 at room temperature for 1 h. After being washed with TBST, the membrane was incubated with SuperSignal West Pico PLUS Chemiluminescent Substrate (34578) from Thermo Fisher Scientific at room temperature for 5 min. Signal was detected on ProSignal ECL Blotting Film (30-507L) from Genesee Scientific. The immunoblotting experiments were repeated three times.

Cell culture

LNCaP and C4-2 cell lines were cultured in Roswell Park Memorial Institute (RPMI) 1640 medium. The LAPC4 cell line was cultured in Iscove's Modified Dulbecco's medium (IMDM). All cell lines were cultured in medium with 10% fetal bovine serum (FBS) and 1% penicillin/streptomycin, incubated in a 5% CO₂ humidified incubator. The cells were cultured in phenol red-free medium with charcoal-stripped FBS for measurements of steroid metabolism. The hypoxic (1% O₂) culture condition was achieved using an O₂/CO₂ incubator (BioSpherix) containing a gas mixture composed of 94% N₂, 5%CO₂ and 1% O₂. The hypoxia-resistant cell lines were established by growing cells under cyclic hypoxia and reoxygenation for several weeks with a gradual increase in hypoxia exposure time. The cells became hypoxia resistant after several passages. RPMI 1640 (10–500), phenol red-free RPMI 1640 (16–500), trypsin (589H100CUST), and PBS (121–500) were obtained from the media preparation core in the Cleveland Clinic Lerner Research Institute. FBS (100–106) and charcoal-stripped FBS (100–119) were from Gemini Bio. All cell lines were routinely authenticated and tested for mycoplasma contamination prior to use. Cells were grown to 70% confluence before transfection with plasmids and siRNA-mediated gene knockdown. Lipofectamine 3000 and Lipofectamine RNAiMAX were used to transfect cells with plasmids and siRNA, respectively, following the manufacturer's protocol. Transfected cells were harvested after 48 h–72 h. Antibiotics were used to select for cells that stably express transfected DNA. *HSD3B1* was knocked out using guide RNA (CGTTTATACTAGCAGAAAGGC) and the virus produced following the LentiCRISPRv2 protocol.⁶⁹

Plasmid construction

The following plasmids were purchased from Sino Biological:

- plasmid pCMV3-OFPSpark-LC3A (HG14322-ANR) expressing N-terminal OFPSpark-tagged *LC3A*
- plasmid pCMV3-HSD3B1-HA (HG14410-CY) expressing C-terminal HA tagged *HSD3B1*
- plasmid pCMV3-HSPA8-Myc (HG11329-CM) expressing C-terminal Myc tagged *HSPA8*
- plasmid pCMV3-ACSS1 (HG12250-UT) expressing *ACSS1*
- plasmid pCMV3-ACSS2-HA (HG22964-CY) expressing C-terminal HA tagged *ACSS2*.

The following plasmids were purchased from GenScript:

- plasmid pcDNA3.1⁺-LAMP2-(K)DYK (OHu23655D) expressing C-terminal Flag-tagged *LAMP2* (transcript variant A)
- Plasmid pCMV3-HSD3B1(1245C)-HA expressing C-terminal HA-tagged *HSD3B1*(1245C) was generated from plasmid pCMV3-HSD3B1-HA (HG14410-CY) by site-directed mutagenesis using the primer GTGGACCGGCACAAGGAGACCCCTGAAGTCC AAGACTCAG and the QuikChange Lightning Multi Site-Directed Mutagenesis Kit (Agilent Technologies, 210515).

Cell viability assay

Cell viability was measured using the CellTiter-Glo 2.0 Cell Viability Assay (G9241) from Promega, following the manufacturer's instructions.

Global protein synthesis assay

Global protein synthesis was measured with the Global Protein Synthesis Assay Kit (ab273286) from Abcam following the manufacturer's instructions.

LDH sequestration assay

LDH sequestration assay was performed following the instruction from MyJoVE Corporation.⁷⁰

LDH enzyme activity assay

LDH enzyme activity was measured with the LDH Assay Kit (Colorimetric, ab102526) from Abcam following the manufacturer's instructions.

Mouse xenograft studies

10^7 cells with 50% Matrigel Basement Membrane Matrix (Corning, 354234) were subcutaneously injected into the right flank of each mouse. Mice were then surgically orchiectomized and implanted with a 5 mg sustained-release DHEA pellet when the tumor volume reached 100 mm^3 . Xenografts were measured 3 times a week using calipers after tumors became palpable. Only the mice with tumor growth were included in statistical analysis.

QUANTIFICATION AND STATISTICAL ANALYSIS

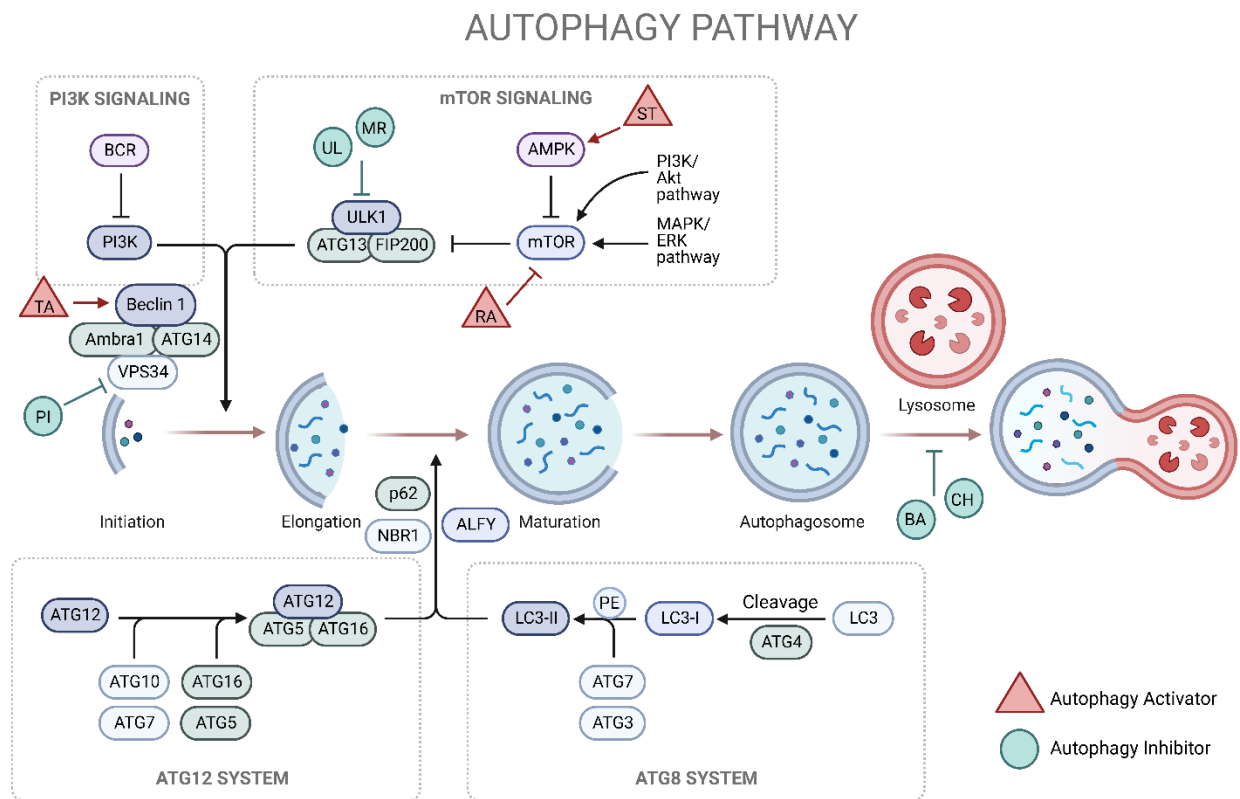
Student t-test analysis was performed to calculate p-value for all the experiments. Additionally, in [Figure 3](#), the tumor volume change was compared using an unpaired two-tailed t test on day 37. Progression-free survival was compared using a log rank (Mantel-Cox) test. The ratio of (T + DHT)/DHEA was compared using a Mann Whitney test. All statistical data analyses were performed in GraphPad Prism 5. * represents $p < 0.05$ and was considered statistically significant. Data are shown as mean \pm SEM. All of the statistical details of experiments can be found in the figure legends.

Cell Reports, Volume 43

Supplemental information

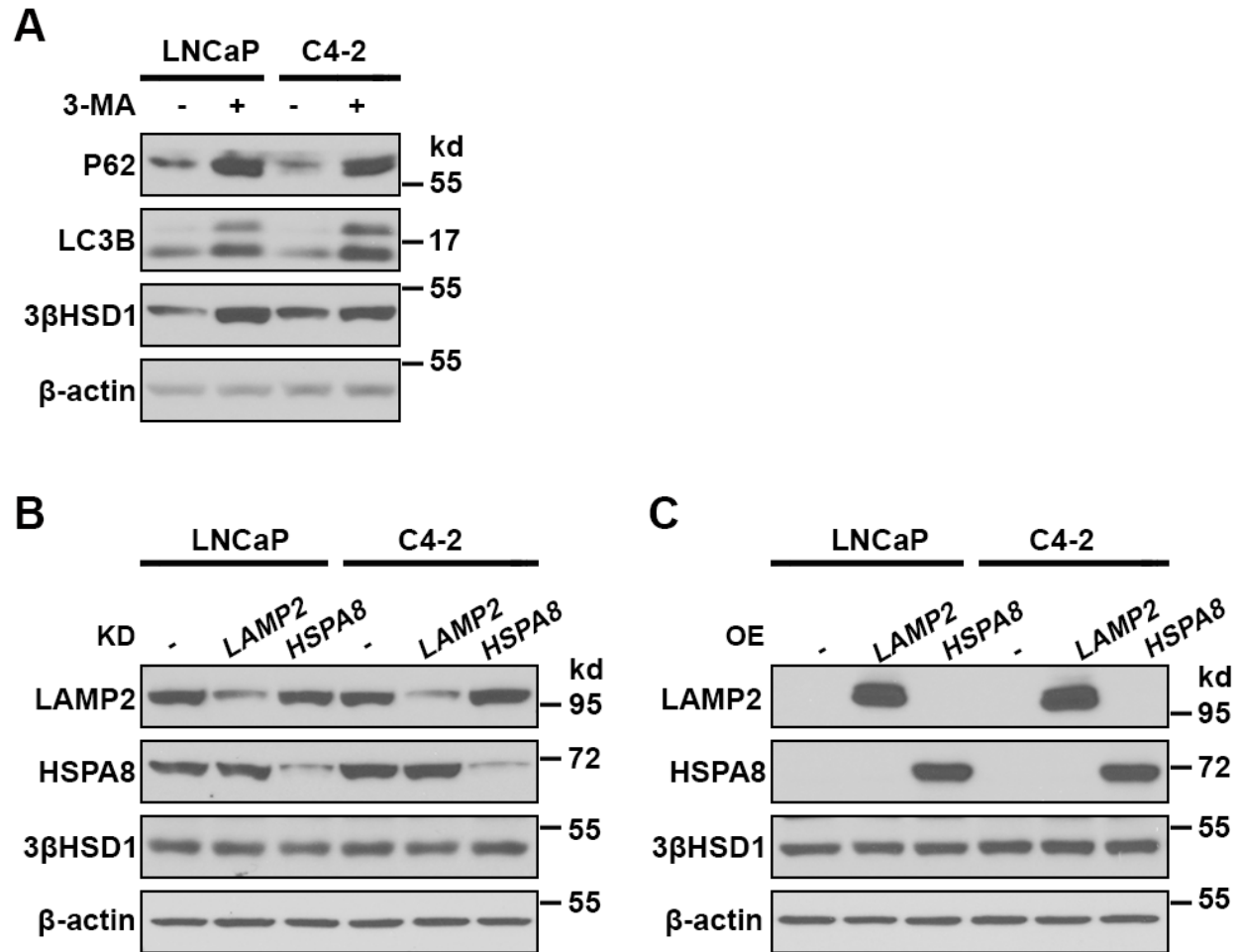
**Chronic hypoxia stabilizes 3 β HSD1
via autophagy suppression**

Liang Qin, Michael Berk, Yoon-Mi Chung, Di Cui, Ziqi Zhu, Abhishek A. Chakraborty, and Nima Sharifi



Supplementary Figure S1 Autophagy pathway and autophagy activators and inhibitors.

The targets of autophagy activators and inhibitors used in Figure 2 are shown.



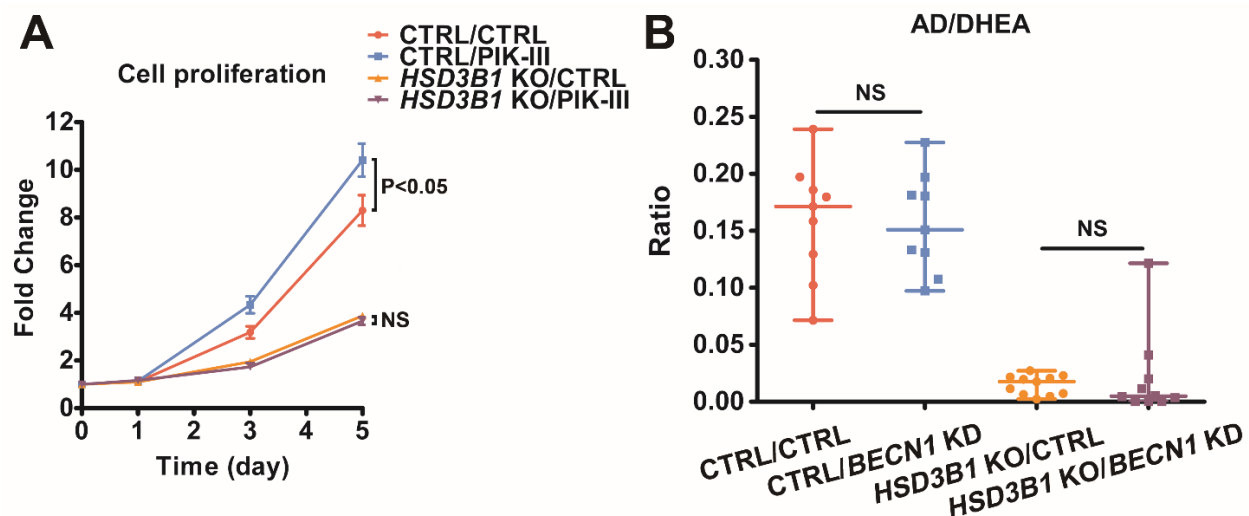
Supplementary Figure S2 Macroautophagy contributes to the degradation of 3βHSD1(367T).

(A) HS cells were treated with 3-methyladenineme (3-MA, 10 mM) for 48 hours.

(B) *LAMP2* was stably knocked down by shRNA in HS cells. *HSPA8* was transiently knocked down by siRNA in HS cells.

(C) *LAMP2-FLAG* and *HSPA8-Myc* were transiently overexpressed in HS cells.

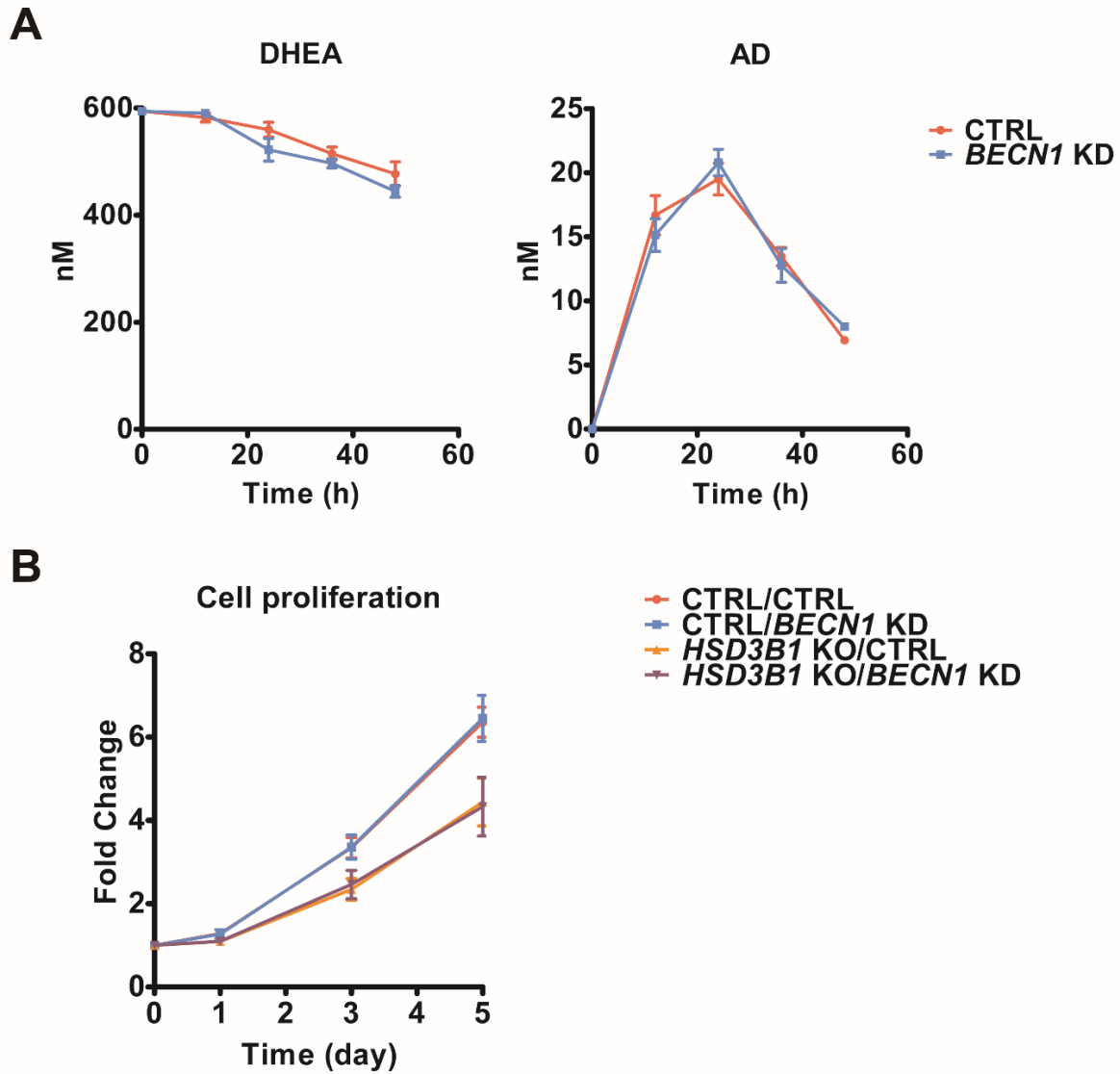
(A-C) P62, LC3B, 3βHSD1, LAMP2, HSPA8, and β-actin proteins were determined by Western blot. β-actin was the loading control. In (C), anti-FLAG antibody was used to detect LAMP2-FLAG protein, and anti-Myc antibody was used to detect HSPA8-Myc protein.



Supplementary Figure S3 The ratio of AD/DHEA is not altered after *BECN1* knock down.

(A) The proliferation of *HSD3B1* knockout (KO) and control C4-2 cells with and without PIK-III (1 μ M) treatment was measured by luciferase assay. The cells were treated with DHEA (50 nM) from time 0. The proliferation was compared using an unpaired two-tailed t test on day 5.

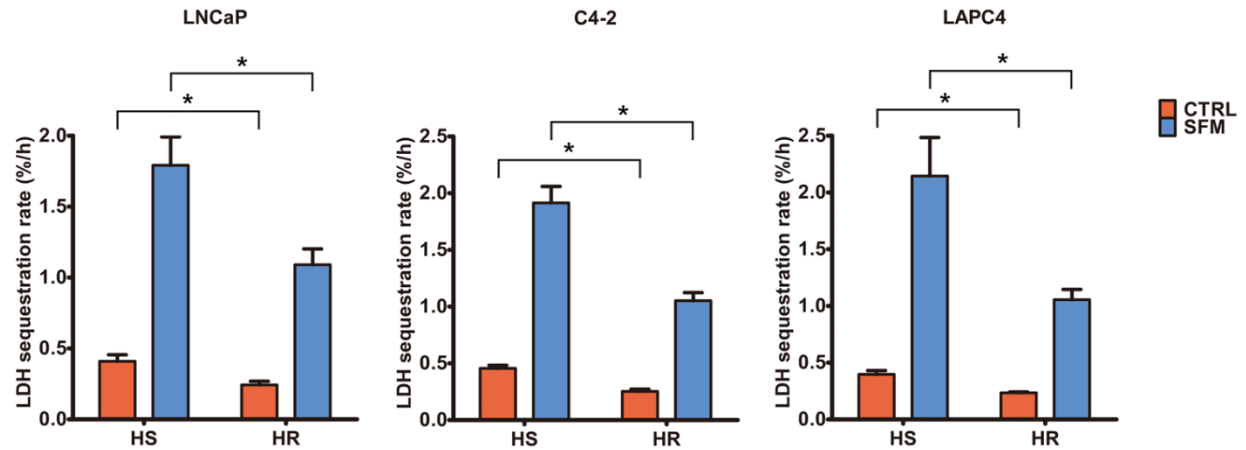
(B) AD and DHEA were measured in xenograft tumor samples from Figure 3C using mass spectrometry, and the ratio of AD/DHEA is shown for each xenograft group. Error bars represent mean \pm SEM.



Supplementary Figure S4 DHEA conversion to AD is not altered by autophagy suppression in LAPC4.

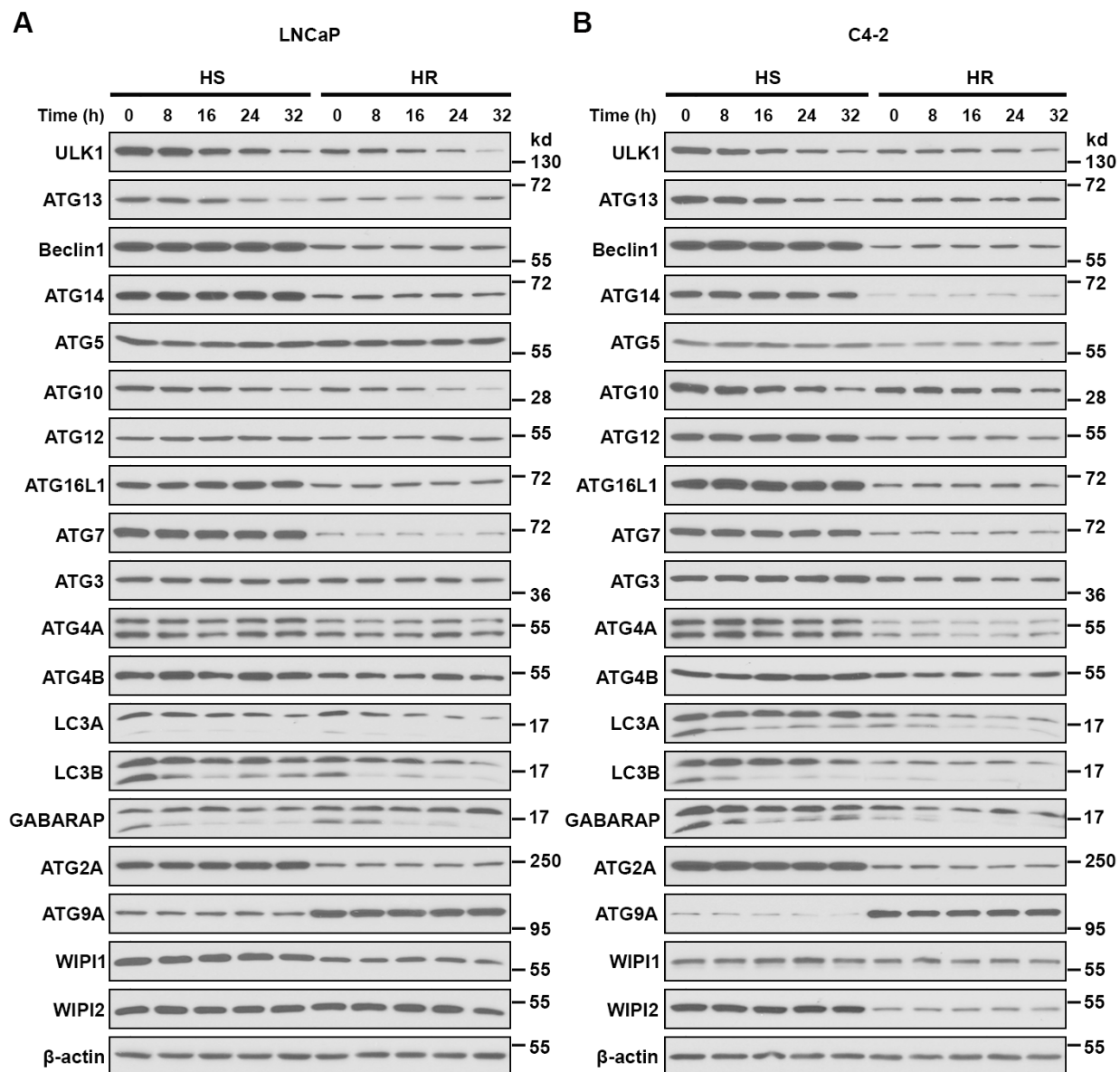
(A) DHEA and AD were quantified by mass spectrometry in LAPC4 cells with *BECN1* stable knockdown and in the control cells. Time 0 represents the point of DHEA addition.

(B) The proliferation of *HSD3B1* knockout (KO) and control LAPC4 cells with and without shRNA-mediated *BECN1* stable knockdown (KD) was measured by luciferase assay. The cells were treated with DHEA (50 nM) from time 0. The proliferation was compared using an unpaired two-tailed t test on day 5.



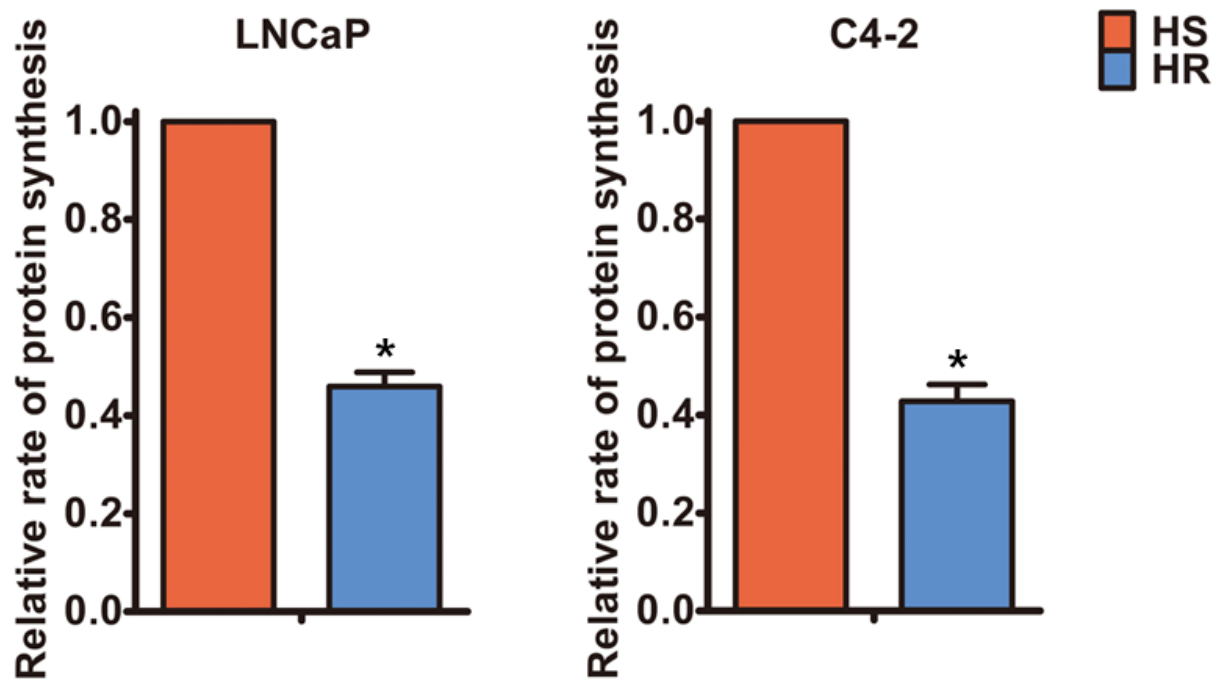
Supplementary Figure S5 Autophagic sequestration is reduced in HR cells under chronic hypoxia.

LNCaP, C4-2, and LAPC4 cells were treated with either normal media (CTRL) or starved with serum-free media (SFM) for 48 hours. Then all the cells were treated with bafilomycin A1 (100 nM) for 3 hours, followed by LDH sequestration assay. LDH activity was quantified from 3 independent experiments. * $P < 0.05$ using a one sample two-tailed t test. Error bars represent mean \pm SEM.



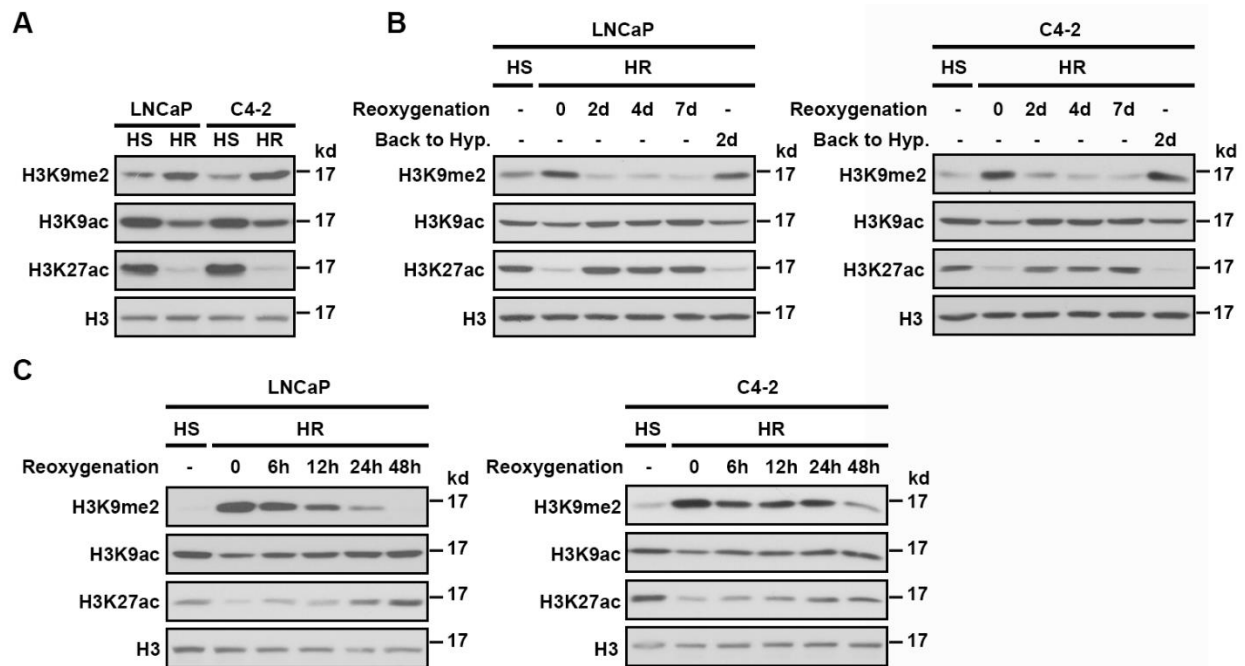
Supplementary Figure S6 The stability of autophagy regulator proteins is unaltered in HR cells.

The stability of the proteins in Figure 4A in HS LNCaP (A) and C4-2 (B) cells under normoxia and HR LNCaP (A) and C4-2 (B) cells under hypoxia was determined by cycloheximide chase stability assay and Western blot. Time 0 represents the point of cycloheximide (50 μ M) addition. β -actin was the loading control.



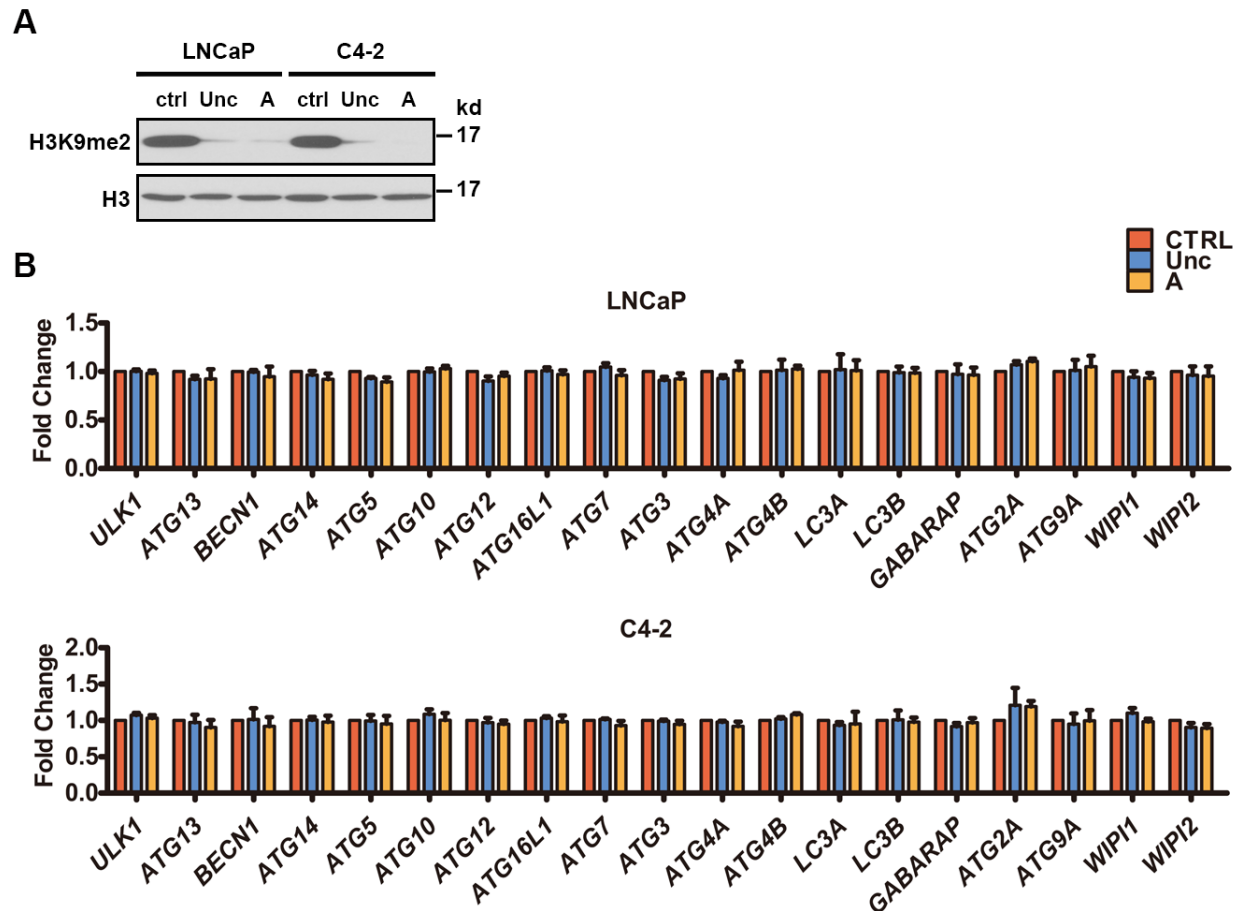
Supplementary Figure S7 HR cells exhibit decreased translation of autophagy-related genes under chronic hypoxia.

The global protein synthesis rate was measured in HS LNCaP and C4-2 cells under normoxia and HR LNCaP and C4-2 cells under hypoxia.



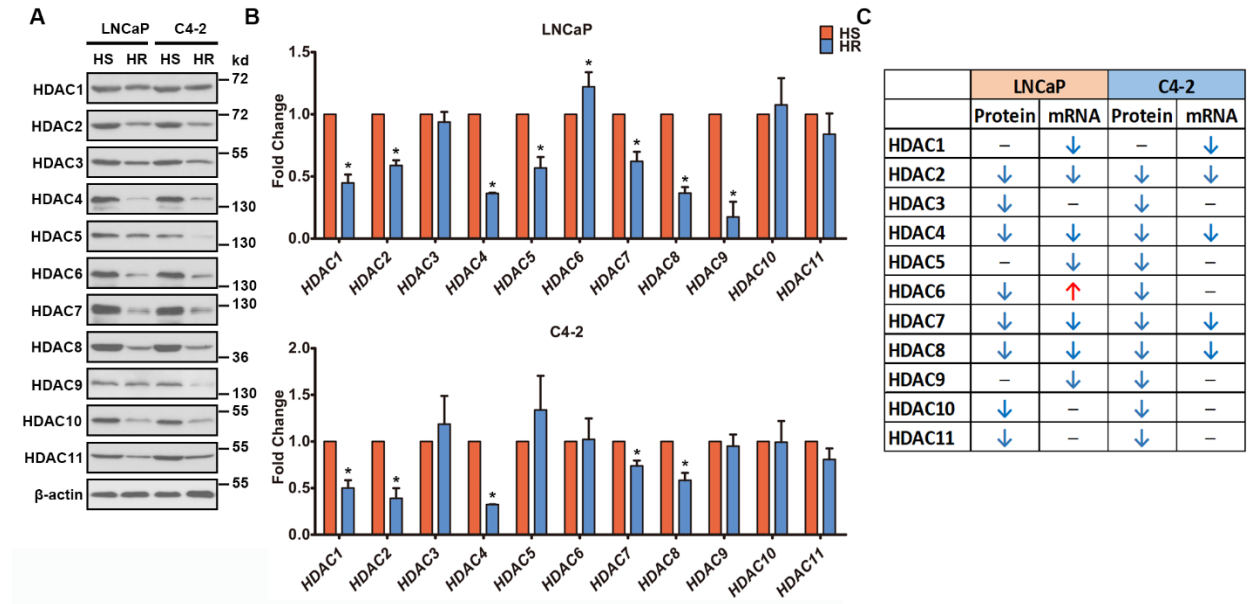
Supplementary Figure S8 HR cells exhibit increased histone methylation and decreased acetylation.

(A-C) H3K9me2, H3K9ac, H3K27ac, and H3 protein was determined by Western blot. H3 was the loading control. (A) Protein expression was determined in HS cells under normoxia and HR cells under hypoxia. (B) Protein expression was determined in HS cells under normoxia and HR cells with and without reoxygenation. “Back to Hyp.” indicates HR cells that, after 7-day reoxygenation, were transferred back to hypoxia for 2 days. (C) Protein expression was determined in HS cells under normoxia and in HR cells with and without reoxygenation.



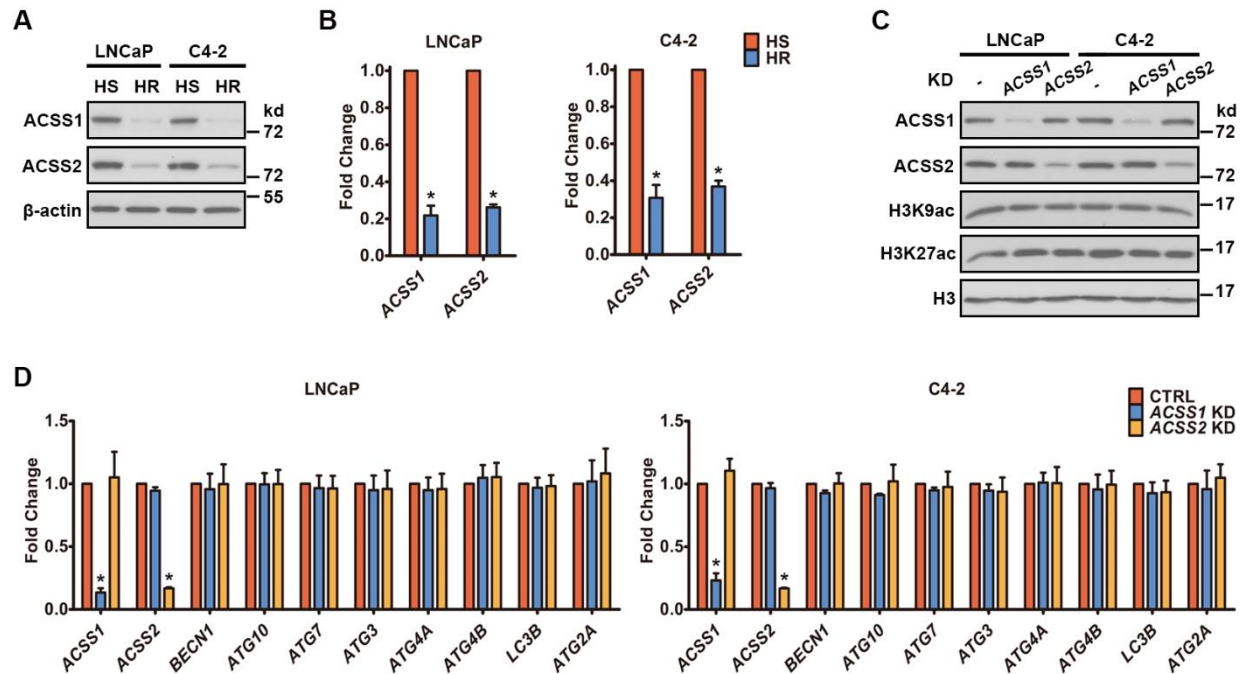
Supplementary Figure S9 Histone methyltransferase inhibitors do not alter the expression of autophagy regulators in HR cells.

(A-B) Both HR LNCaP and C4-2 cells were treated with the methyltransferase inhibitors UNC0642 (UNC, 5 μ M) or A-366 (A, 20 μ M) for 36 h under hypoxia. (A) H3K9me2 and H3 protein was determined by Western blot. H3 was the loading control. (B) mRNA was determined by qPCR for the indicated autophagy regulators. *ACTB* was the loading control. Error bars represent mean \pm SEM.



Supplementary Figure S10 HDAC expression is not altered in HR cells.

(A-B) HDAC1-11 and β -actin protein (A) and mRNA (B) were determined by Western blot (A) and qPCR (B) in HS cells under normoxia and HR cells under hypoxia. β -actin was the loading control. * $P < 0.05$ using a one sample two-tailed t test. Error bars represent mean \pm SEM. Results in (A) and (B) are summarized in Table (C).



Supplementary Figure S11 Single knockdown of either *ACSS1* or *ACSS2* cannot alter the transcription of autophagy regulators.

(A-B) *ACSS1*, *ACSS2*, and β -actin proteins (A) and mRNA (B) were determined by Western blot (A) and qPCR (B) in HS cells under normoxia and HR cells under hypoxia. β -actin was the loading control.

(C-D) *ACSS1* or *ACSS2* were stably knocked down by shRNA in HR cells. (C) *ACSS1*, *ACSS2*, H3K9ac, H3K27ac, and H3 protein was determined by Western blot. H3 was the loading control.

(D) *ACSS1*, *ACSS2*, *BECN1*, *ATG10*, *ATG7*, *ATG3*, *ATG4A*, *ATG4B*, *LC3B*, and *ATG2A* mRNA was determined by qPCR. *ACTB* was the loading control. * $P < 0.05$ using a one sample two-tailed t test. Error bars represent mean \pm SEM.